Structure, dynamics, and the electronic absorption of benzene–argon clusters

Laurence E. Fried and Shaul Mukamel
Department of Chemistry, University of Rochester, Rochester, New York 14627

(Received 19 February 1991; accepted 24 September 1991)

We present a new method for calculating cluster absorption spectra using classical molecular dynamics and simulated annealing techniques. We then apply this method to benzene–Ar clusters. Cluster absorption spectra are shown to be dominated by an inhomogeneous distribution of isomer absorptions. The absorption spectrum of each isomer, however, results from the interplay of structure, fluctuations, and dynamics. We find that accompanying the solid to liquid transition, there is a spectroscopic transition from a periodic to a decaying autocorrelation function of the electronic energy gap. Benzene–Ar clusters are found to undergo transitions from a solid to a 2D liquid to a 3D liquid as the number of Ar atoms is increased from 1 to 21 at 20 K.

I. INTRODUCTION

Molecular and atomic clusters have been a subject of extensive experimental[1–9] and theoretical investigation.[10–29] Clusters play an important role in nucleation and catalysis. On a more fundamental level, clusters represent a bridge between condensed phase systems and isolated molecules. It is therefore important to ask what analogs of condensed phase behaviors exist in clusters, and what behaviors are unique to clusters (such as magic numbers[1]).

Recent interest in the analogs of a bulk phase transition in a finite cluster was initiated by the work of Berry and coworkers,[11–16] who have proposed that it is possible for finite clusters to have separate melting and freezing temperatures. Between the melting and freezing temperature is a coexistence regime, where segments of a trajectory at fixed energy show liquidlike or solidlike behavior. This picture has been confirmed by classical molecular dynamics simulations of Ar clusters.[13] Phase coexistence depends on the presence of a potential minimum with low energy relative to other potential minima.[14] This can lead to dramatic size dependence; Ar_7 shows phase coexistence whereas Ar_8 does not.[14] Pure Ar clusters can exhibit strikingly sharp phase transitions. For instance, Amar and Berry[13] found a dramatic jump in the rms bond fluctuation δ for Ar_{13} as the energy was changed by a fraction of the Lennard-Jones well depth. Pure Ar clusters have been studied through properties that have clear macroscopic analogs, such as caloric curves,[13] as well as properties most often used to characterise the dynamics of small systems, such as isomerization rates, fractal dimensions, power spectra, and the K entropy.[15] Freeman and Doll have studied quantum mechanical effects in the melting of Ar clusters.[18]

In a recent examination of temperature-dependent cluster spectra, Hahn and Whetten[4] have studied size-resolved benzene–Ar_N clusters. They found that spectra with N between 18 and 25 showed both broad (FWHM$\approx$30 cm^{-1}) and sharp (FWHM$\approx$5 cm^{-1}) spectral features. Hahn and Whetten were able to obtain some temperature control by changing the preparation conditions of the clusters. The spectral features did not shift with temperature, and the sharp features became dominant as the temperature was decreased. These observations were suggested to support the picture of phase coexistence with the sharp and broad features resulting from solidlike and liquidlike configurations, respectively. Very recently Schmidt *et al.*[8] have reported the absorption spectrum of benzene–Ar clusters in the size range $N=1$ to 9. They used an improved two-color technique which is less susceptible to cluster fragmentation (providing better control of cluster size) than the one-color technique used by Hahn and Whetten.

Bösiger, Knochenmuss, and Leutwyler[3] have studied size-resolved carbazole–Ar_N clusters. They conducted a Monte Carlo calculation of the temperature at which a rare gas atom can first cross the plane of the carbazole as a function of the number of argon atoms. This behavior is called a "side-crossing transition." Bösiger *et al.* found that as N was increased, the clusters moved from non-side-crossing to side-crossing configurations. This N dependent transition correlated well with an increase in the experimental FWHM as a function of N. Knochenmuss and Leutwyler[30] have conducted a hole burning study of carbazole–Ar clusters. They were able to burn a hole in the narrow absorption feature which persisted for at least 50 ns, but were unable to burn a hole in the broad absorption feature. This suggests that the underlying cluster relaxations in the narrow feature are slower than in the broad feature. Even, Ben-Horin, and Jortner[6] have studied the electronic absorption spectrum of size-resolved dichloroanthracene–Kr_N and dichloroanthracene–Ar_N clusters. They found that the spectrum is sharp at $N=1$, but becomes broad and featureless at $N=11$. They interpret this behavior in terms of a wetting–nonwetting transition from two dimensional configurations to three dimensional configurations. Interestingly, at $N=17$, sharp spectral features once again appear. This change was assigned to a nonrigid 3D to rigid 3D transition.

Previous theoretical work on rare gas clusters containing a chromophore molecule has centered upon several problems. There have been attempts[19,20] to explain the spectral shift of chromophore–rare gas clusters via Longuet-Higgins–Pople theory[21] and semiempirical electronic structure calculations.[22] An electrostatic model taking into account

 0021-9606/92/010116-20$06.00

intermolecular electronic overlap was used by Ben-Horin, Even, and Jortner[23] to calculate the ionization potential of large van der Waals molecules. Penner *et al.*[9] have compared experimental results on the radiative lifetime and spectral shift of dichloroanthracene–Ar, Kr, and Xe clusters with the predictions of a classical electrostatic model.[24] Leutwyler and Bösiger[2] have performed Monte Carlo simulations of carbazole–Ar clusters. They studied how cluster configurations and rms bond fluctuations changed with the number of Ar atoms and temperature.

There has also been previous theoretical work on benzene–Ar clusters in particular. Hahn[5] conducted a Monte Carlo simulation of benzene–Ar clusters. She classified various cluster geometries and looked at how the rms bond fluctuations varied with temperature. More recently, Adams and Stratt[25] have conducted a Monte Carlo simulation of benzene–Ar_{19} and Ar_{19} clusters. By examining the distribution of instantaneous normal mode frequencies they found that the presence of the benzene in the cluster made the solid to liquid phase transition less sharp. They suggested that cluster configurations with the benzene external to the rest of the cluster might be responsible for the observed spectra. Schmidt *et al.*[8] very recently reported Monte Carlo simulations of benzene–Ar_2 clusters in conjunction with rotationally resolved spectra.

In a preliminary report of some of the work presented here[26] we simulated the absorption spectrum of benzene–Ar_N clusters. In this work we first generated a sampling of the Boltzmann distribution of cluster configurations by conducting multiple independent annealings. This allowed us to examine the relative probability of various isomers. The time scales of cluster motion were studied, something that cannot be done within the framework of Monte Carlo simulations. We concluded that the electronic absorption is dominated by inhomogeneous broadening resulting from multiple cluster configurations and that solidlike clusters can have both broad and sharp spectral features.

In this paper we give a full presentation of our semiclassical method for calculating the absorption spectrum of a cluster. We then use this method to calculate the absorption spectrum of benzene–Ar clusters at several values of N and at several temperatures. We examine several possible criteria for characterizing benzene–Ar clusters as liquid or solid and find that they do not always agree. We find several interesting phase transitions, and look at their spectroscopic signatures. In particular, we find that benzene–Ar_N clusters at 20 K undergo a transition from solid at $N = 1$ to a two dimensional liquid at $N = 2, 4$, and then change to a 3D liquid as N increases from 10 to 21. We also look closely at the role of diffusion, large amplitude cluster motions, the time scale of cluster motions, and cluster structure in determining the observed spectra. Corresponding to these structural transitions, we identify *spectroscopic transitions* as the absorption moves between several limiting cases that we identify. These spectroscopic transitions signify qualitative changes in the dynamics of the difference between the potential energy surfaces $\hat{U} \equiv V_g(t) - V_e(t)$ along a trajectory.

The rest of this paper is organized as follows: Section II derives the line shape formula used in the calculations and then discusses the static and dynamical properties used to characterize the clusters. In Sec. III we discuss the results of our calculations. Our conclusions are given in Sec. IV.

II. THEORY

A. The electronic absorption line shape

In this section we derive and motivate the procedure used to calculate the cluster electronic absorption spectrum. We use a method similar to the semiclassical spectral density theory of Islampour and Mukamel.[28] The normalized absorption line shape within the Condon approximation can be written in a time-dependent form:

$$I(\omega) = \mathrm{Re}\int_0^\infty dt\, \mathrm{Tr}\left[e^{i(\omega + H_g)t}\rho_g e^{-iH_e t}\right], \tag{1}$$

where

$$H_g = \sum_i \frac{p_i^2}{2m_i} + V_g(\{q_i\}), \tag{2}$$

$$H_e = \sum_i \frac{p_i^2}{2m_i} + V_e(\{q_i\}) + E_e, \tag{3}$$

$$\rho_g = e^{-H_g/kT}/\mathrm{Tr}\left[e^{-H_g/kT}\right]. \tag{4}$$

Here H_g is the ground state adiabatic Hamiltonian of the chromophore–cluster system, H_e is the excited state adiabatic Hamiltonian, and ρ_g is the equilibrium density matrix. Equation (1) can be rewritten in terms of the dynamics of the electronic energy gap $\hat{U} \equiv V_g - V_e$:

$$I(\omega) = \mathrm{Re}\int_0^\infty dt\, e^{i(\omega - E_e)t}\left\langle \exp_-\int_0^t dt'\,\hat{U}(t')\right\rangle, \tag{5}$$

$$\hat{U}(t) \equiv e^{iH_g t}\hat{U}e^{-iH_g t}, \tag{6}$$

where $\exp_-$ is the negative time ordered exponential

$$\exp_-\left[i\int_0^t dt'\,\hat{U}(t')\right] \equiv 1 + i\int_0^t dt'\,\hat{U}(t') + i^2\int_0^t dt'\int_0^{t'} dt''\,\hat{U}(t'')\hat{U}(t') + \cdots. \tag{7}$$

$\langle\cdots\rangle$ refers to the thermal expectation value. Equation (5) is exact, but requires knowledge of the quantum dynamics of $\hat{U}(t)$. We consider here classical approximations to Eq. (5). In the classical limit the expectation value in Eqs. (1) and (5) becomes an integral over phase space. $\hat{U}(t)$ becomes the classical function $U(q)$ propagated forward a time t on the ground state potential energy surface. ρ_g becomes a phase space distribution $\rho_g(p_0, q_0)$. The effects of zero point motion may be approximately included by using the Wigner function of the quantum thermal density matrix instead of the classical phase space distribution. These replacements yield

$$I(\omega) = \int dp_0\, dq_0 \left\{\mathrm{Re}\int_0^\infty dt \exp\left[i\int_0^t dt'\, U(q_0[t'])\right] \times e^{i(\omega - E_e)t}\rho_g(p_0, q_0)\right\}, \tag{8}$$

where $q_0[t]$ denotes the coordinate of the phase point (q_0,p_0) propagated forward a time t by classical dynamics. Thus, in the classical limit each phase point can be thought of as having its own spectrum. The observed spectrum is the sum of the trajectory spectra, with each point weighted by the thermal probability $\rho_g(q_0,p_0)$.

The above formula is exact in the *static limit*, when molecular motions are slow compared to the dephasing time (inverse absorption linewidth). We then get

$$I_s(\omega) = \int dp_0\, dq_0\, \delta[\omega - E_e - U(q_0)]\rho_g(p_0,q_0). \tag{9}$$

Equation (8) is also exact if V_g and V_e are displaced harmonic oscillators. Substantial statistical variations between the spectra associated with various trajectories in Eq. (8) can make a direct evaluation of Eq. (8) quite difficult. In the present work, we lessen these variations by making use of a cumulant expansion. This accomplishes the goal of averaging phase factors before exponentiation, thus avoiding the famous "sign problem" in Monte Carlo sampling.[27]

Let us define

$$I(t) = \left\langle \exp_- i\int_0^t dt'\,\hat{U}(t') \right\rangle. \tag{10}$$

This is also equal to

$$I(t) = \left\langle \frac{i}{t_a}\int_0^{t_a} dt_0 \exp_- \int_0^t dt'\,\hat{U}(t'+t_0) \right\rangle, \tag{11}$$

where t_a is an "averaging time." It is important to note that Eq. (11) is correct regardless of the value of t_a. In practice we will choose t_a to be long compared to the dephasing time, and very long compared to typical molecular vibrations (hundreds of vibrations). It is then appropriate to think of the integral over t_0 as a microcanonical sampling. We introduce a cumulant expansion for $I(t)$ as expressed in Eq. (11) by writing $I(t) = \langle e^{-f(t)}\rangle$, and then expanding $f(t)$ in powers of $\hat{U}$. This yields to second order in $\hat{U}$

$$\begin{aligned} f(t) = & -i\int_0^t dt'\langle\hat{U}(t')\rangle_t \\ & -\int_0^t dt'\int_0^{t'} dt''\langle\hat{U}(t'')\hat{U}(t')\rangle_t \\ & +\frac{1}{2}\left[\int_0^t dt'\langle\hat{U}(t')\rangle_t\right]^2, \end{aligned} \tag{12}$$

where $\langle A\rangle_t \equiv \int_0^{t_a} dt_0\, A(t_0)/t_a$. The above assumptions regarding the length of t_a imply that $\langle\hat{U}(t')\rangle_t$ is independent of t'. Defining $\lambda = \langle\hat{U}\rangle_t$, we have

$$f(t) = -i\lambda t + \int_0^t dt'\int_0^{t'} dt''\langle U'(t'')U'(t')\rangle_t, \tag{13}$$

where $U' \equiv \hat{U} - \lambda$.

In the classical limit, the expectation value in Eq. (11) becomes an integral over all of phase space. λ becomes a phase space function $\lambda(p_0,q_0)$, whereas $\langle U'(t)U'(0)\rangle_t$ becomes a classical autocorrelation function. This yields

$$I(\omega) = \mathrm{Re}\int dp_0\, dq_0 \int_0^\infty dt \exp\{i[\omega - E_e + \lambda(q_0,p_0)]t - g(t,q_0,p_0)\}\rho_g(q_0,p_0), \tag{14}$$

$$g(t,q_0,p_0) \equiv \int_0^t dt' \int_0^{t'} dt''\, J(t'',q_0,p_0), \tag{15}$$

$$J(t,q_0,p_0) \equiv \langle U'(q_0)U'(q_0[t])\rangle_t. \tag{16}$$

Here λ represents a *spectral shift* and g is responsible for the *spectral line shape*. The absorption spectra of clusters are dominated by their multiple configurations. This often leads to highly structured inhomogeneous contributions. Inhomogeneous broadening is exactly incorporated in Eq. (14) through the phase space integration over p_0 and q_0, where each phase point is associated with its own spectrum. Homogeneous contributions to the spectrum enter through the line shape function $g(t,q_0,p_0)$. The calculations of Islampour and Mukamel were based on a second order cumulant expansion of the *entire* line shape. That calculation predicts a Gaussian inhomogeneous line shape. The present formulation provides a rigorous treatment of inhomogeneous broadening, which is essential for a realistic simulation of benzene–Ar clusters. From now on, we shall call the line shape associated with a particular initial condition a *subspectrum*. The total spectrum is a thermally weighted average of the subspectra.

Under the present formula, each subspectrum is symmetric around $\omega = E_e - \lambda$. This will clearly lead to unphysical spectra at low temperature. We incorporate asymmetry into the line shape by introducing a thermal correction factor.[28] Introducing $\tilde{J}(\omega) = 1/2\pi\int dt \exp(i\omega t)J(t)$, we have the semiclassical relation

$$\tilde{J}(\omega) = [1 + \tanh(\omega/2kT)]\tilde{J}_C(\omega), \tag{17}$$

where $\tilde{J}_C(\omega)$ is the classical power spectrum of $U'(t)$ calculated along a trajectory. The thermal correction factor used here may be derived by expanding $I(t)$ to second order in U, and then applying the fluctuation–dissipation relation between the positive and negative frequency components of $\langle J(\omega)\rangle$, as outlined by Yan and Mukamel.[31]

Let us consider some important limiting cases of Eq. (14). Below, we use these limiting cases to explain the observed spectra.

Case I [*Periodic* $J(t)$]. If $J(t) = \Delta^2\cos(\omega t)$ then the spectrum predicted by our line shape formula will be a set of sharp peaks spaced by ω. The FWHM of each peak is equal to zero, regardless of Δ^2 or ω.

Case II [*Damped* $J(t)$]. Consider the case where the autocorrelation of U' relaxes irreversibly. We shall represent it as $J_C(t) = \Delta^2 f(t/\tau_c)$, where $f(0) = 1$ and τ_c is a characteristic time scale. Henceforth, we define

$$\Delta \equiv \sqrt{J_C(0)}. \tag{18}$$

In the limit of high temperature and fast relaxation the line shape becomes a Lorentzian, with FWHM equal to $2\Delta^2\tau_c$.

Case III [*Static* $J(t)$]. If atomic motions are slow compared to the inverse of the absorption linewidth (dephasing time), then the semiclassical theory predicts a Gaussian line shape with a FWHM equal to 2.35Δ. The

line shape then becomes independent of cluster dynamics. The static approximation has been widely used to calculate electronic absorption spectra. A good example is the recent work on the line shape of the solvated electron.[32] The static approximation is not usually appropriate for benzene–Ar clusters.

The width of the spectrum when Case II holds is often narrower than when Case III holds. This effect is called *motional narrowing*,[33] since relaxation of $J(t)$ leads to a narrowing of the absorption line shape with increasing relaxation rate. Below, we will see that motional narrowing plays an important role in producing the absorption spectra of benzene–Ar clusters. Further insight into these cases can be obtained by considering a Brownian oscillator model for nuclear dynamics.[34] This model is exactly soluble and interpolates between the various limiting cases.

B. Properties studied

Below we examine the relation between the benzene–Ar absorption spectrum and characteristics of the cluster. We have studied the following cluster properties.

1. Diffusion coefficients

One of the main motivations for studying clusters is to determine the extent to which finite systems display bulk properties. The classification of clusters as being "liquidlike" or "solidlike" is therefore an interesting idea.[11] One possible way of distinguishing between liquid and solid clusters is by calculating an average diffusion constant of the cluster atoms along a trajectory. Consider the average displacement of the N Ar atoms in the cluster:

$$\langle r^2(t)\rangle \equiv \frac{1}{t_a}\sum_{i=1}^{N}\int_0^{t_a} dt_0 |r_i(t+t_0)-r_i(t_0)|^2, \qquad (19)$$

where $r_i(t)$ is the position of Ar atom i in a frame which moves with the overall rotation of the cluster. We have used the rotating frame described by Jellinek and Li[35] for the purposes of evaluating the cluster diffusion coefficient. This provides a means of eliminating the effects of cluster rotation. The angular velocity of this rotating frame is defined by the relation

$$\omega(t) \equiv I^{-1}(t)L, \qquad (20)$$

where L is the cluster angular momentum and $I(t)$ is the instantaneous moment of inertia tensor. We numerically integrated the angular velocity of the frame $\omega(t)$ to determine quaternion parameters[36] describing the orientation of the frame at every point in time.

We calculated cluster diffusion coefficients via the relation

$$D = \frac{1}{6}\frac{\langle r^2(t_1)\rangle - \langle r^2(t_0)\rangle}{t_1 - t_0}, \qquad (21)$$

where t_1 and t_0 were chosen to be in the range where $\langle r^2(t)\rangle$ was a linear function of time. In our studies, we have found that there is a wide range of times where $\langle r^2(t)\rangle$ depends linearly with t. Prior to this linear regime, $\langle r^2(t)\rangle$ depends quadratically with t, whereas after the linear regime $\langle r^2(t)\rangle$ saturates. In the studies reported below it sufficed to choose $t_1 = 5$ ps and $t_0 = 3.5$ ps.

2. rms bond fluctuations

rms bond fluctuations constitute another quantity we use to distinguish between solidlike and liquidlike clusters. The rms bond fluctuation (commonly referred to as δ) is defined by the relation

$$\delta = \frac{1}{N(N-1)}\sum_{i<j}\left[\frac{\langle r_{ij}^2\rangle_t - \langle r_{ij}\rangle_t^2}{\langle r_{ij}\rangle_t^2}\right]^{1/2}, \qquad (22)$$

where the expectation value refers to an average along a trajectory. Since δ is based on bond distances rather than absolute position, it is not necessary to employ a rotating frame in its calculation.

In our calculations we restrict the sum over i and j to only Ar atoms. Thus, δ is a measure of the amplitude of the Ar–Ar motion. The Lindemann criterion states that solids generally have δ values less than 0.1, while liquids generally have δ values greater than 0.1. This criterion has also shown to have validity for clusters.[13]

Let us consider how the liquid or solid nature of a cluster calculated on the basis of δ will differ from calculations based on the diffusion coefficient. δ reflects the overall amplitude of the Ar motion. The diffusion constant D, on the other hand, reflects the existence of "wandering" motions in the cluster. Thus, a cluster showing a large amplitude periodic motion will have a vanishing diffusion constant, but could still possibly be characterized as a liquid by the Lindemann criterion. On the other hand, a cluster where some Ar's wander while others are fixed will have a nonzero diffusion constant, and will thus be characterized as a viscous liquid (viscous because the diffusion constant is low). The rms bond fluctuations, however, could very conceivably remain low because only a subset of the bonds show substantial fluctuations. The two criteria are therefore complementary.

In the calculations presented below we find that as the temperature T is increased, liquidlike behavior as characterized by D usually sets in before liquidlike behavior as characterized by δ. In some cases (e.g., $N = 16$ and $N = 21$) this is because Ar atoms bound to the edge of the benzene are fairly free to wander, while Ar atoms bound to the surface of the benzene form a tight packing configuration. This is an example of solidlike and liquidlike motions "coexisting" in different regions of the cluster.

3. Fluctuation of the energy gap

Another measure of the amplitude of the cluster motion is the fluctuation of the electronic energy gap U. This quantity (which we call Δ) is equal to

$$\Delta = \sqrt{\langle U^2\rangle_t - \langle U\rangle_t^2}. \qquad (23)$$

The expectation value in Eq. (23) refers to an average over a trajectory. The rms bond fluctuation δ is a natural measure of the amplitude of molecular motion. Δ, however, is a measure of the *spectroscopic importance* of molecular motions. Large amplitude molecular motions will not produce broad spectra unless Δ is sufficiently large. In the static limit, the FWHM of a subspectrum is equal to 2.35Δ. Thus, the corre-

lation of the FWHM with Δ is a sensitive probe of the importance of dynamics in producing the spectrum. When the FWHM is significantly less than 2.35Δ, the line is motionally narrowed, as discussed above. Δ is rigorously equal to the second moment of the subspectrum, so correlating the FWHM with Δ is a measure of how well the second moment describes the spectrum (i.e., the extent to which the spectrum is like a Gaussian).

Sue *et al.*[37] have given a Padé approximant which smoothly interpolates between the static and motional narrowing limits. Given the relaxation time τ of $J_C(t)$ and Δ, the FWHM Γ is given by

$$\Gamma = \Delta \frac{2\Delta\tau + 2.676(\Delta\tau)^2}{1 + 0.966\Delta\tau + 1.136(\Delta\tau)^2}. \tag{24}$$

In the present work, we take the time scale of relaxation to be the inverse of the average frequency ω_{avg} defined below. The agreement of the FWHM with the Padé formula is expected to be good if $J_C(t)$ is a decaying function of arbitrary time scale.

4. Average frequency of the motion

Another important measure of solvent motion is the average frequency of the motion. The power spectrum of any dynamical property can be used as a probability distribution in determining the average frequency of the motion. We use the power spectrum of $U'(t)$, since the spectrum is determined by the dynamics of U'. Thus, we define the average frequency by

$$\omega_{\text{avg}} = \frac{\int_0^\infty d\omega\, \omega |U'(\omega)|^2}{\int_0^\infty d\omega |U'(\omega)|^2}. \tag{25}$$

The average frequency of the motion is useful in determining the effect of the time scale of cluster motions on the width of spectral features. In particular, we show below that clusters exhibiting low frequency motions often have broad spectra. This is predicted by the model of a damped $J(t)$ (Case II). The average frequency of the motion is also a useful diagnostic in determining how the time scale of solvent motion changes with temperature in a thermal ensemble, or how relevant time scales change with the number of Ar atoms.

5. Cluster asymmetry number

The absorption spectrum of benzene–Ar clusters can be profoundly affected by cluster structure. One important way of characterizing the structure of clusters is by the cluster asymmetry number:

$$z \equiv \left| \left\langle \sum_i \text{sgn}(r_i \cdot C_6) \right\rangle_t \right| / N, \tag{26}$$

where r_i is the position vector of Ar atom i, and C_6 is a unit vector along the C_6 axis of the benzene molecule. The origin in Eq. (26) is taken to be the center of mass of the benzene. When $z = 1$ the benzene lies on the surface of the cluster whereas $z = 0$ for a symmetric cluster. The value of z can also provide some valuable dynamical information. When side crossing does not take place, then N times the asymmetry number is equal to an integer. Its deviation from an integer value is thus a signature of side crossing motion.

III. RESULTS

A. Calculation of the line shape

In order to calculate the absorption line shape of the cluster, we must specify the ground state and excited state potential surfaces V_g and V_e. We took the benzene molecule to be rigid but not fixed, thus neglecting intramolecular vibrations. This is a common approximation in molecular dynamics.[36] The ground state potential consisted of a standard pairwise additive Lennard-Jones carbon–argon and hydrogen–argon parametrization that has been successfully applied to other conjugated chromophore/rare gas clusters.[29] Similarly, we used an empirical excited state potential function. Since the first excited state of benzene has only modest charge separation, it was natural to take a Lennard-Jones form (thus neglecting charge-induced dipole interactions). We were able to approximately match the experimental spectral shifts by keeping the excited state potential the same as the ground state potential, except for the Ar–H σ and the Ar–C ϵ.

Figure 1 shows the ground and excited state Ar–H and Ar–C potential surfaces, as well as the Ar–Ar potential, which was taken to be the same in the ground and excited state. $U_{\text{Ar-C}} \equiv V_g(\text{Ar–C}) - V_e(\text{Ar–C})$ is always positive, and thus always produces a redshift. Test calculations have shown that the inclusion of only $U_{\text{Ar-C}}$ leads to a redshift that increases smoothly with the number of Ar atoms N. The experimental results,[4] on the other hand, show an initial doubling in the redshift from $N = 1$ to $N = 2$, and then a small decrease with N up to about $N = 21$.

We were able to match this behavior by the inclusion of the $U(\text{Ar–H}) \equiv V_g(\text{Ar–H}) - V_e(\text{Ar–H})$ term. As is shown

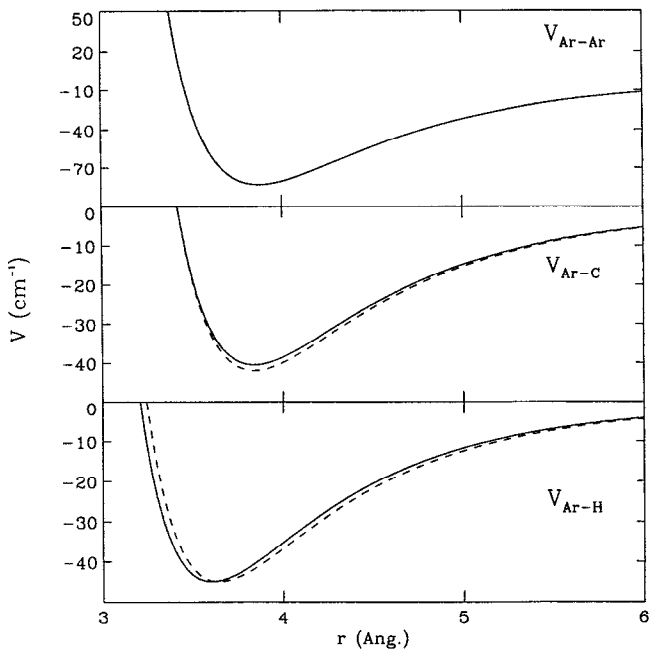

FIG. 1. Excited and ground state pair potentials used. Solid line: ground state potential; dashed line: excited state potential.

TABLE I. Lennard-Jones parameters used in the simulation.

Parameter	Ground state	Excited state
$\epsilon_{Ar\,Ar}$	83.17 cm^{-1}	83.17 cm^{-1}
$\sigma_{Ar\text{-}Ar}$	3.45 Å	3.45 Å
$\epsilon_{Ar\text{-}C}$	40.42 cm^{-1}	41.87 cm^{-1}
$\sigma_{Ar\text{-}C}$	3.42 Å	3.42 Å
$\epsilon_{Ar\text{-}H}$	45.00 cm^{-1}	45.00 cm^{-1}
$\sigma_{Ar\text{-}H}$	3.21 Å	3.24 Å

in Fig. 1, $U_{Ar\text{-}H}$ produces a redshift at large distances and a blueshift at small distances. For the $N=1$ and $N=2$ clusters the Ar atoms are usually located at the center of the benzene ring. For larger N the Ar atoms can come closer to the H atoms, thus decreasing the overall redshift. We found that this balancing of attractive and repulsive interactions was necessary to approximate the experimental pattern of spectral shifts. The potential parameters used are given in Table I.

Initial conditions corresponding to a Boltzmann distri-

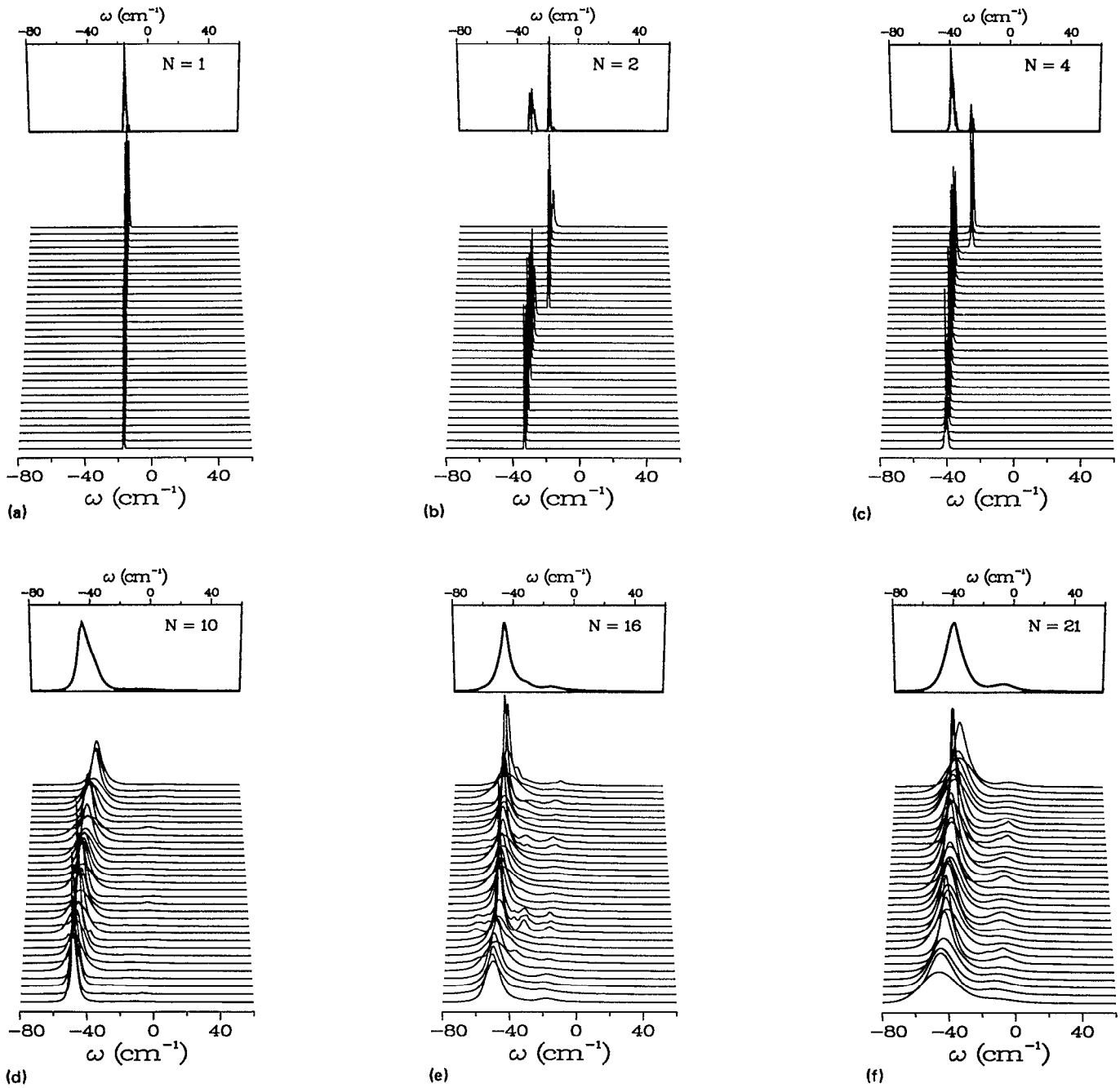

FIG. 2. Calculated absorption spectra and subspectra at $T=20$ K for various Ar numbers (N). The frequency scale is shifted so that $\omega=0$ corresponds to the absorption of the isolated benzene.

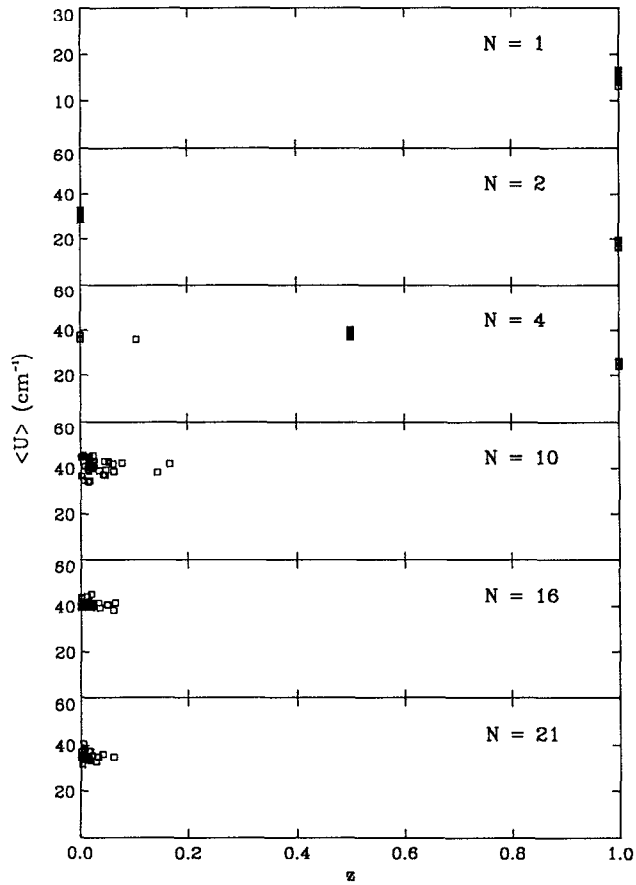

FIG. 3. Correlation between $\lambda \equiv \langle U \rangle$ and the cluster asymetry number z.

bution at a given temperature were generated by a staged classical Monte Carlo annealing procedure.[38] Following the annealing, a molecular dynamics calculation was undertaken to find the cluster absorption spectrum. The annealing began at a temperature of 100 K. The stages used were $T = 40$, 30, 20, 10, 5, and 2.5 K. An independent annealing run was done for each initial condition. This was necessary because clusters often have many isomers separated by significant barriers. During the annealing, a confining sphere about the benzene was imposed by adding an extra term to the potential

$$V_{\text{sphere}}(r) = (r/r_c)^{20}. \tag{27}$$

The radius of the sphere was taken to be equal to 15 Å. During the annealing procedure the benzene was fixed. This does not represent an approximation, because any one particle may be fixed in a Monte Carlo simulation without affecting the results, since the integrand depends only on distances between particles. In the molecular dynamics portion of the calculation, however, the benzene was allowed to move. Annealing runs of successively more Monte Carlo cycles were done until the average internal energy among the runs was unchanged upon doubling the number of cycles. The number of cycles required to achieve equilibration varied greatly with N. 65 000 cycles were sufficient to equilibrate $N = 1$ clusters at 20 K. To equilibrate the $N = 21$ clusters at 2.5 K took 500 000 cycles. For each spectrum, 32 independent annealing runs were done. Initial velocities were chosen from a classical thermal distribution at the given temperature. The center of mass velocity of the entire cluster was set to zero at the beginning of the molecular dynamics calculation. The clusters did, however, have nonzero angular momentum.

Subspectra corresponding to each run were generated by a 140 ps constant energy molecular dynamics simulation. We used the Bulirsch-Stoer adjustable step size rational extrapolation integration algorithm described in *Numerical Recipes*.[39] The energy was conserved to seven digits throughout the calculation. The motion of the benzene was described by center of mass and quaternion parameters. At 35 fs intervals the energy gap U was evaluated. The average of $U(t)$ along the trajectory (denoted λ) was calculated, and then used to find $U'(t) = U(t) - \lambda$. A small exponential damping was applied to the $U'(t)$ values, which were then Fourier transformed to give $J_C(\omega) = |U'(\omega)|^2$. The purpose of the exponential damping was to avoid "edge effects" in the Fourier transform. The iterated trapezoid rule was used to do all numerical integrals. Once $J_C(\omega)$ was found, the quantity $J(t)$ was calculated via Eq. (17). The line shape was then calculated by using Eq. (14). A small Gaussian damping was added to the final Fourier transform over t to enhance the convergence of the integral. The 140 ps trajectories we ran were long enough to resolve a spectral feature of FWHM 0.3 cm^{-1} within the present numerical scheme.

B. Size dependence of cluster dynamics and spectra

Cluster absorption spectra have most commonly been studied at fixed preparation conditions with the number of Ar atoms N varied. In this subsection we report a set of calculations done at a temperature of 20 K for N values from 1 to 21. We will compare the results of our calculations to the experimental spectra. It is important to remember, however, that there are a number of uncertainties that make direct comparison with experiment difficult. To begin with, the temperature at which the experiments[4,8] were performed is not precisely known. While our use of the temperature 20 K is reasonable, we note that the cluster spectra are very sensitive to temperature. A second point for consideration is that not enough is known about the cluster preparation conditions to be sure that an equilibrium Boltzmann distribution of clusters is generated in the experiment. Finally, cluster fragmentation after the absorption of the second photon is very possible. The recent two-color experiments of Schmidt *et al.*[8] allow the amount of cluster fragmentation to be decreased. Two color experimental results, however, are currently available only in the size range $N = 1$ to 9, whereas one color results are available in the size range $N = 1$ to 40.

Despite these uncertainties, we have been able to reproduce many of the qualitative trends and features seen in the experimental spectra. Figure 2 shows the spectra calculated by the procedure outlined in the last subsection. In our calculations a double peaked structure appears at $N = 2$ and $N = 4$, which then disappears at $N = 10$. This is in close agreement with recent experiments, which also show a double peaked structure which begins to disappear at $N = 9$. Experiments show that the more shifted peak ("A," in the

notation of Schmidt *et al.*) has approximately twice the spectral shift of the "B" peak. We have a similar ratio of spectral shifts. Also, our calculations show that the spectral shift of the B band is approximately equal to the $N = 1$ spectral shift. This feature is also born out experimentally. Schmidt *et al.* assigned these features to an inhomogeneous distribution of isomers in the $N = 2$ cluster, with the A band coming from asymmetric cluster with both Ar atoms on the same side of the benzene. Referring to the subspectra shown in Fig. 2, we see that the calculated A and B bands are due to an inhomogeneous distribution of isomers with different spectral shifts. In Fig. 3 we show the correlation between the spectral shift of a subspectrum and the cluster asymmetry number. This clearly confirms the assignment of Schmidt *et al.* Recall that clusters that do not undergo side crossing have rational asymmetry numbers. By inspection of Fig. 3, we see that no side crossing occurs when $N = 1$ and 2. Only one side crossing occurs at $N = 4$. Side crossing becomes common, however, at $N = 10$, 16, and 21. In the language of cluster phase transitions, a 2D to 3D transition occurs between $N = 4$ and $N = 10$.

In the experiments of Hahn and Whetten[4] there is a pronounced appearance of sharp spectral features beginning at about $N = 18$. We also find a similar appearance of sharp spectral features. When $N = 10$ the FWHM of the total spectrum is 11.1 cm^{-1}. At $N = 16$, however, the FWHM of the spectrum has decreased to 7.6 cm^{-1}. At the same time, a prominent sideband to the red of the main peak appears when $N = 16$. This is similar to the coexistence of broad and sharp spectral features found by Hahn and Whetten.

The coexistence of broad and sharp spectral features has been a subject of much interest, especially with regard to the question of phase coexistence. In the calculations presented below, we elucidate the role of structure and dynamics in producing broad and sharp spectral features. In Fig. 4 we consider the correlation between the FWHM of a subspectrum and the cluster diffusion constant of the underlying motion. When $N = 1$ (not shown), all trajectories have zero diffusion constant. This is indicative of a solidlike cluster. When $N = 2$ we find that some trajectories have zero diffusion constant, while others have a nonzero diffusion constant. Both isomer types ($z = 0$ and $z = 1$) have diffusive and nondiffusive trajectories. At $N = 4$, the population of nondiffusive clusters has decreased, and floppy clusters become more prevalent. Only one trajectory, however, demonstrates side crossing. The $N = 4$ cluster could be usefully characterized as a 2D liquid. Two-dimensional rigid and fluxional states of carbazole–Ar clusters have been studied by Leutwyler and Bösiger.[2] As N is further increased, the average diffusion constant decreases. In the terminology of bulk liquids, one would say that the clusters become more viscous.

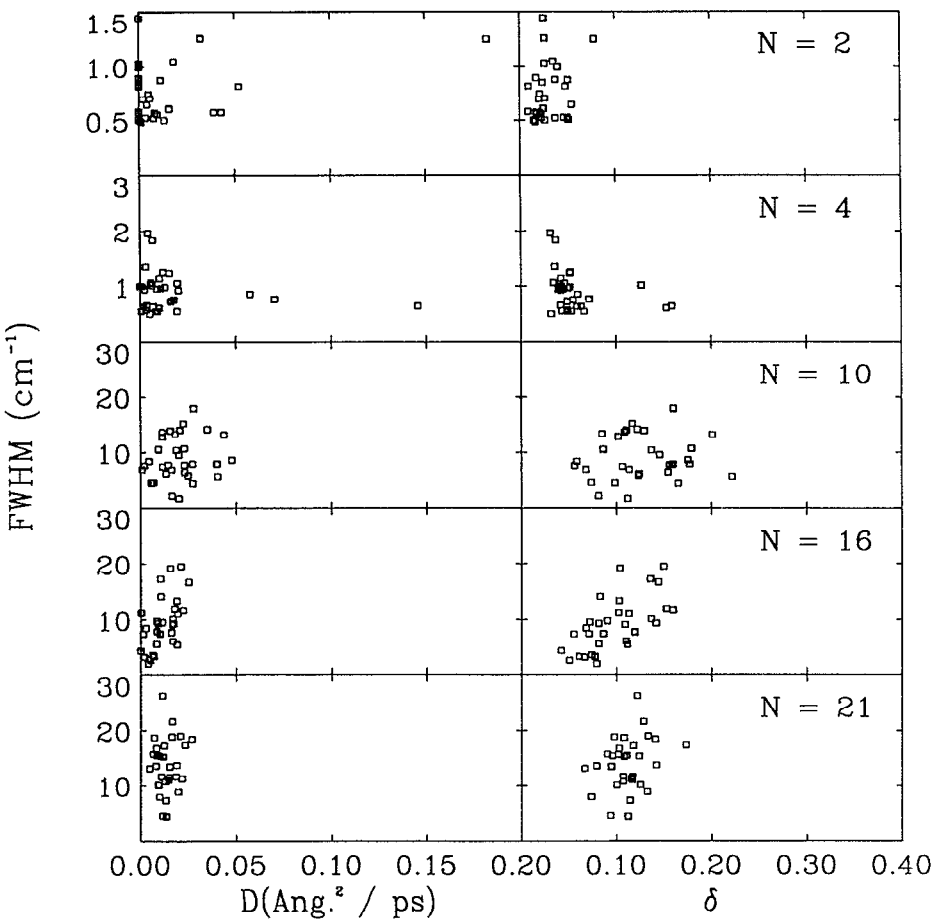

FIG. 4. Left column: the correlation between the cluster diffusion constant D and the FWHM of the subspectra. Right column: the correlation between the rms bond fluctuation δ and the FWHM of the subspectra.

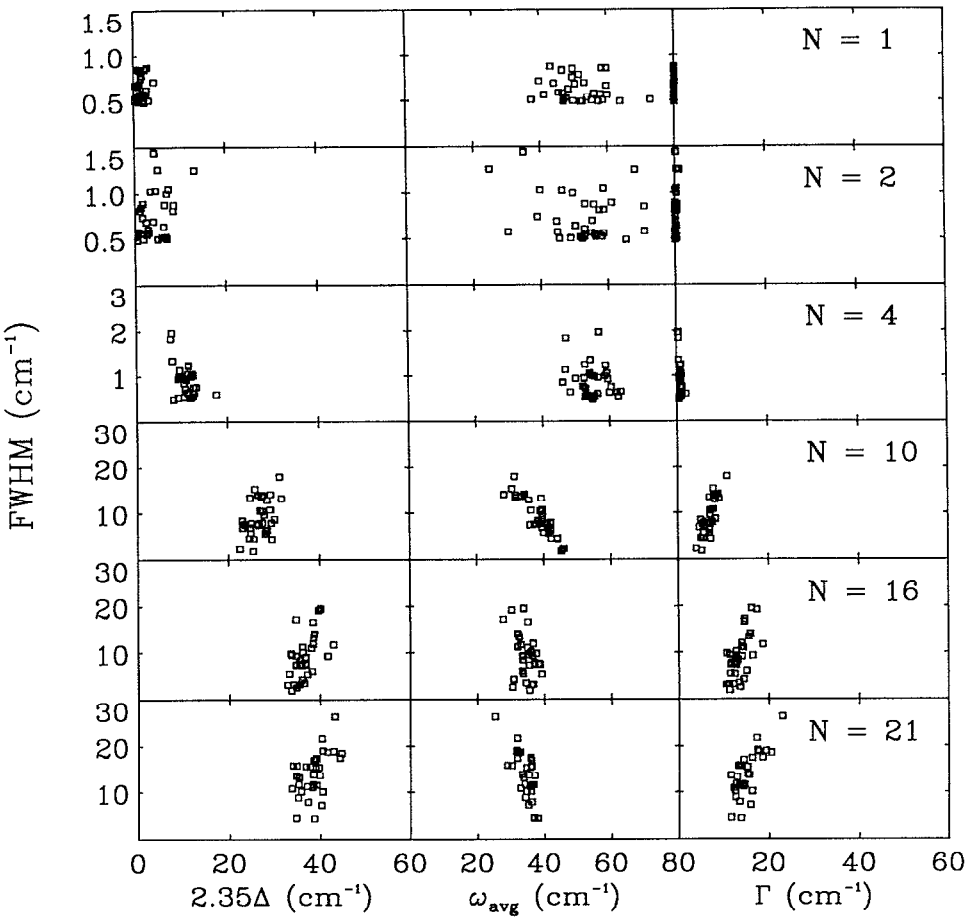

FIG. 5. Left column: the correlation between the rms fluctuation of $U(t)$ (Δ) and the FWHM of a subspectrum for various N at 20 K. Middle column: the correlation between the average frequency of the motion (ω_{avg}) and the FWHM of a subspectrum. Right column: the correlation between the Padé formula Γ for the FWHM and the calculated FWHM.

On an intuitive level, one would probably expect that diffusive clusters would have much broader spectra than nondiffusive clusters. When viewed as a function of N, this is patently untrue. While the cluster diffusion constant decreases from $N = 10$ to $N = 21$, the FWHM of the subspectra increases very rapidly. This is because the larger clusters have much larger fluctuations in the energy gap, although its average (λ) increases only slowly with N. Within a particular N value, it is only sometimes true that nondiffusive clusters lead to significantly narrower spectra than diffusive clusters. For the $N = 10$ and $N = 16$ clusters there is a noticeable correlation between D and the FWHM. This correlation is much less apparent when $N = 2$, 4 or 21, however.

This situation underlines the difference between the finite cluster and a true liquid–solid phase transition in a bulk system. The true solid is characterized by a zero diffusion coefficient. Usually there is only one (or at most a few) forms a crystal structure takes. Thus, the combination of few configurations and nondiffusive motion leads to sharp spectral lines. A liquid, on the other hand, is characterized by a high degree of configurational disorder and a nonzero diffusion constant. When the temperature is raised, the diffusion constant suddenly jumps from a zero to a nonzero value as the solid melts. This is often accompanied by a sudden broadening of spectral lines. This bulk behavior can be contrasted with benzene–Ar clusters. As N is varied, there is no sudden jump in the diffusion constant.

The rms bond fluctuation δ is another important quantity describing the underlying cluster motion. The Lindemann criterion states that systems with δ values less than 0.1 are usually solids, whereas systems with δ values greater than 0.1 are usually liquids. δ is a measure of the overall amplitude of the motion, whereas the diffusion constant measures the presence of wandering motions in the cluster. Figure 4 also shows the correlation between δ and the FWHM of the associated subspectrum. The overall trends in the δ values as a function of N follow the trends seen in the diffusion constant. The $N = 2$ clusters have δ much less than 0.1. As N is increased δ first increases then decreases.

There are some important differences, however, between the solid and liquid nature of the clusters as defined by the Lindemann criterion and as defined by D. According to the Lindemann criterion, the $N = 2$ cluster is a solid; according to the diffusion constant, there exists both solid and liquid forms in the thermal ensemble. This discrepancy is due to the fact that there is no unique definition of a phase in a finite system. Other differences also exist. The $N = 21$ cluster has δ values indicating a coexistence of solidlike and liquidlike forms. Its diffusion constant, however, is more representative of a viscous liquid.

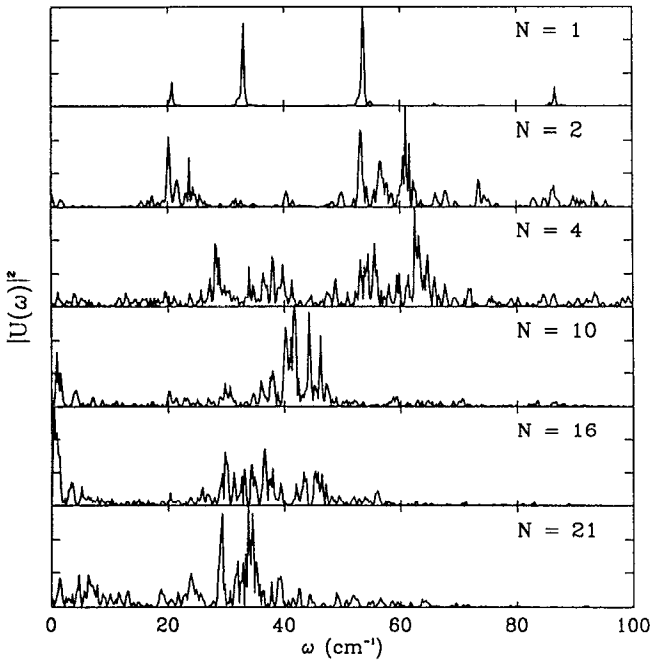

FIG. 6. Typical power spectra $U(\omega)^2$ calculated along a single trajectory for various cluster sizes at 20 K.

Next, let us consider the correlation between δ and the FWHM of a subspectrum. This correlation measures the extent to which large amplitude cluster motions lead to broad spectra. The right half of Fig. 4 shows that for the $N = 10$, 16, and 21 clusters there is a clear correlation between the amplitude of the underlying nuclear motion and the FWHM of the associated subspectrum. The distribution of FWHM and δ values, however, are both unimodal. Thus, there is no separation into distinct liquid and solid "phases" possible based on the δ criterion.

δ is a measure of the amplitude of the Ar motions. A good measure of the spectroscopic significance of the Ar motions, however, are the fluctuations of $U(t)$. In Fig. 5 we plot the calculated FWHM as a function of Δ. In the static limit (Case III) the FWHM becomes equal to 2.35Δ. Thus, the correlation between Δ and the FWHM is a measure of how important dynamics are in determining the isomer subspectra. To begin with, we note that 2.35Δ is always an overestimate of the FWHM. This is a manifestation of motional narrowing (Case II) or periodic motion (Case I). As N increases, the FWHM becomes more nearly equal to 2.35Δ. This implies that cluster motions are becoming less important in determining the subspectra as N increases; the subspectra *themselves* are becoming inhomogeneous lines. (Recall that the total spectrum is an inhomogeneous distribution of subspectra.) This is due to an increasing width of the subspectra (thus decreasing the spectroscopically relevant time scale of cluster motion), as well as a slowing of the cluster motions, as shown below.

In the middle panel of Fig. 5, we consider the correlation between the FWHM of a subspectrum and the average frequency of the cluster (ω_{avg}), as defined in Eq. (25). First we note that the average frequency decreases monotonically with N. This is because more low frequency collective modes become available as N increases. Second, note that ω_{avg} is inversely correlated with the FWHM of a subspectrum for $N = 10$, 16 and $N = 21$. This effect results from motional narrowing. The correlation between the FWHM and the average frequency is not always good; an example of this is found when $N = 1$, 2, and 4. The lack of a dependence of the FWHM on ω_{avg} and the poor accuracy of the static approximation suggests that the system is in the Case I limit of a periodic $J_C(t)$ when $N = 1$, 2, and 4.

In the right panel of Fig. 5 we show the correlation between the actual FWHM and the simple estimate of the FWHM (Γ), the Padé approximant formula of Eq. (24). This measures the extent to which the line shape can be accounted for by a decaying $J_C(t)$ of arbitrary time scale. For the $N = 1$, 2, and 4 clusters, the inclusion of the motional narrowing mechanism leads to much better agreement with the experimental FWHM. The independence of the FWHM on ω_{avg}, however, suggests that it is better to describe $J_C(t)$ as being periodic in these cases. For N equal to 10, 16, and 21 Γ is a very good predictor of the calculated FWHM; the model of a decaying $J_C(t)$ becomes very good.

The absorption line shape is completely determined by the autocorrelation of the energy gap $J_C(t)$. It is most convenient to study this quantity through its Fourier transform $|U'(\omega)|^2$. We show the $|U'(\omega)|^2$ associated with a subspec-

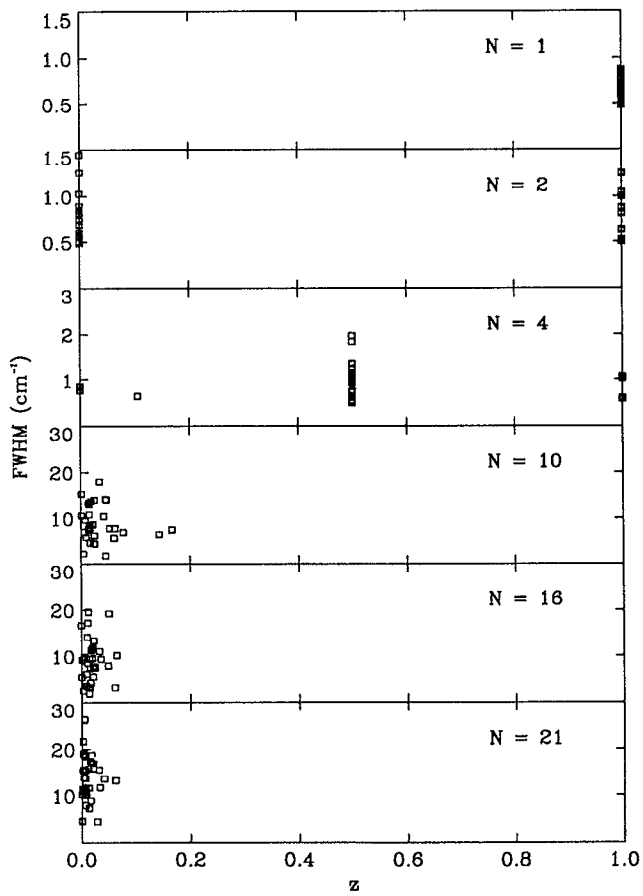

FIG. 7. Correlation between the asymmetry number and the FWHM of a subspectrum for various cluster sizes at 20 K.

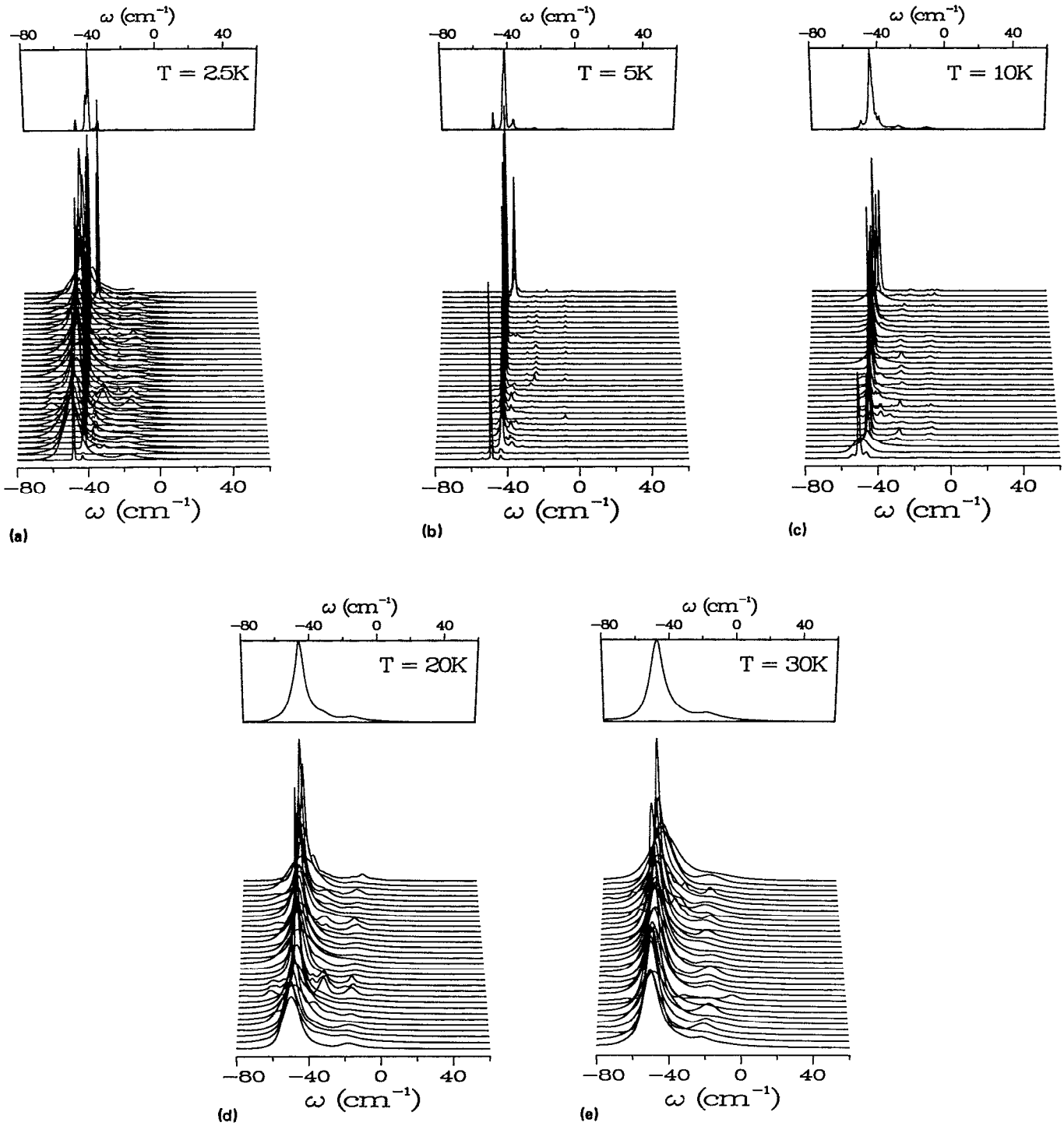

FIG. 8. Spectra and subspectra for the $N = 16$ cluster at various temperatures.

trum randomly chosen from the 32 initial conditions used in our simulation in Fig. 6. At $N = 1$ there are only four peaks in $|U'(\omega)|^2$; this corresponds to a periodic $J_C(t)$ (Case I). For N equal to 10 and 16 there is substantial amplitude near zero frequency. This is characteristic of a damped function in time, so a transition has been made to Case II. This means that the solid ($N = 1$) to liquid transition as a function of N is reflected by the presence (liquid) or absence (solid) of low frequency modes in $|U'(\omega)|^2$.

We have so far considered the role of diffusion, fluctuations, and cluster frequencies in producing the observed spectra. Cluster structure is of course another important factor determining the observed spectrum. In Fig. 7 we show the correlation between the absolute value of the cluster

asymmetry number, as defined in Eq. (26), and the FWHM of the subspectra. As noted above, the $N=1$, 2 and (with one exception) 4 clusters show no side crossing. The $N=2$ and 4 clusters display noninterconverting isomers. Figure 7 shows that there is no correlation between the FWHM of a subspectrum and the isomer type for $N=2$ and $N=4$. For $N=10$, 16, and 21 side crossing motions of the Ar atoms occur. This leads to a distribution of asymmetry numbers, as opposed to a limited number of fractional asymmetry numbers. Also, as N is increased, the maximum asymmetry of the cluster decreases. Adams and Stratt suggest that states with benzene on the surface of the cluster may be responsible for the sharp spectral features seen for intermediate ($N=18...23$) sized clusters. Based on our calculations, we do not find such configurations to be very probable. There is no clear correlation between the FWHM of the subspectra and the asymmetry number. In particular, partial extrusion of the benzene from the center of the cluster does not produce exceptionally narrow spectral features. Highly asymmetric clusters are not found in our calculations.

Let us summarize the main conclusions of this subsection:

(1) The clusters undergo a solid to liquid transition as N is increased from 1 to 21. The exact point of transition depends on the criterion used to define liquid or solid. Diffusion can exist when the rms bond fluctuation is well under 0.1.

(2) The static approximation always overestimates the FWHM of the subspectra. This behavior is predicted by the motional narrowing (Case II) or periodic motion (Case I) paradigms discussed above. Based on the dependence of the FWHM on the ω_{avg}, we find that the periodic motion paradigm is best for small N. The motional narrowing paradigm, however, is best for larger N ($N=10$, 16 and 21), which suggests a damped $J(t)$.

(3) The $N=1$, 2, and 4 clusters do not undergo side crossing transitions. Side crossing occurs for $N=10$, 16, and 21. As N increases the clusters become more symmetric. Partially asymmetric clusters with a number of Ar atoms on both sides of the benzene do not have narrower absorptions than symmetric clusters.

C. Cluster spectra vs T: $N=16$

Experiments on rare gas–chromophore systems are most commonly carried out at fixed preparation condition for various N's. Phase transitions in bulk systems, however, are most commonly studied as a function of temperature. This motivates the study of a single cluster size at various values of the temperature. Hahn and Whetten have performed studies of benzene–Ar clusters for different preparation conditions, which offers a certain degree of temperature control. We elucidate the role of temperature in inducing phase transitions and spectral changes for the $N=16$ cluster here. Below we calculate spectra at a wide range of temperatures. We note that the ground state distribution used is entirely classical; consequently zero point energy is not included and thus the vibrational structure of the subspectra may be underestimated at very low temperatures.

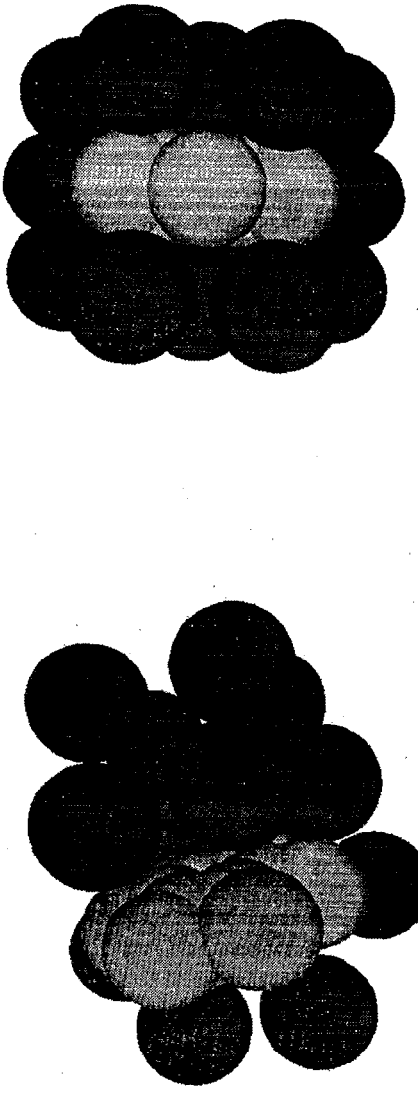

(a)

(b)

FIG. 9. Configurations for the $N=16$ cluster at high and low temperature: (a) 2.5 K, (b) 30 K.

In Fig. 8 we show the calculated absorption spectrum and associated subspectra for the $N=16$ cluster at various temperatures. The spectrum evolves from a set of very sharp peaks at 2.5 K, to a sharp peak on top of a broader background at 20 K. The broad background grows while the sharp peak broadens at 30 K. At 10 K there is a bimodal distribution of subspectra widths; most subspectra are sharp (FWHM $<5\ \text{cm}^{-1}$), with three relatively broad subspectra found (FWHM $>10\ \text{cm}^{-1}$) (Also see Fig. 10.) As the temperature increases, broad subspectra become increasingly common and the bimodal nature of the subspectra distribution disappears.

Cluster configurations at 2.5 and 30 K are shown in Fig. 9. At 2.5 K we have chosen a highly symmetric isomer.

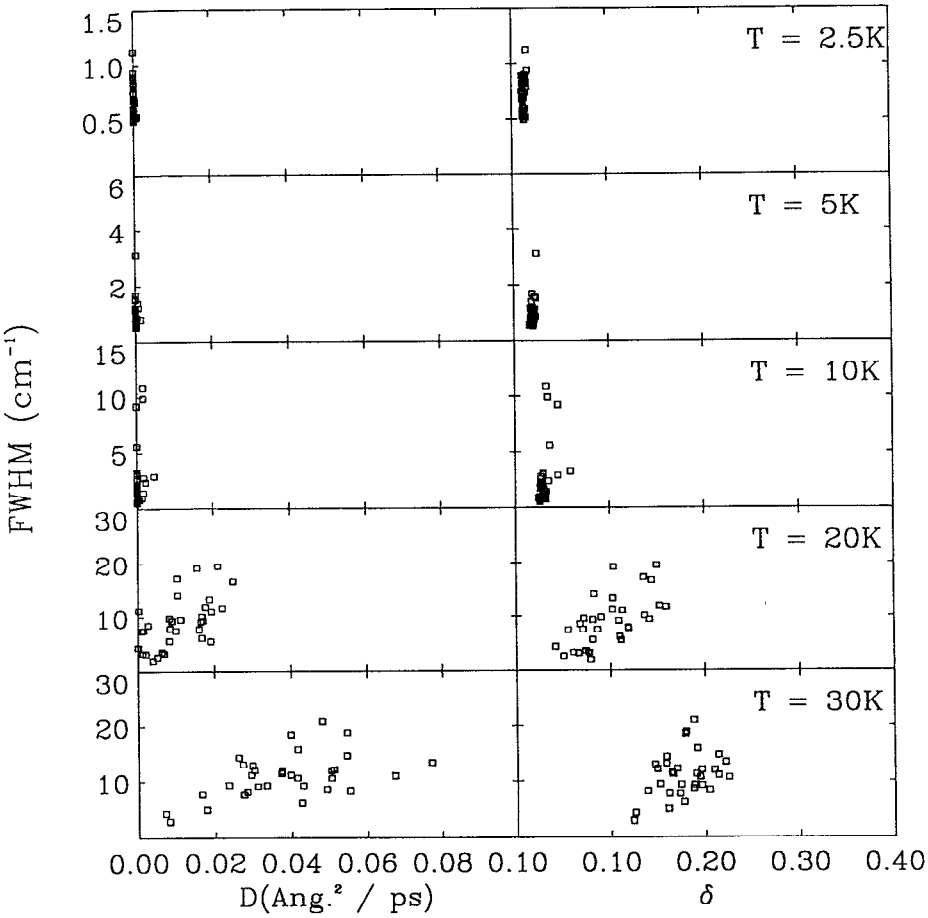

FIG. 10. Indicators of the solid-liquid transition for the $N = 16$ cluster. Left column: correlation between the cluster diffusion constant D and the FWHM of a subspectrum. Right column: correlation between the rms bond fluctuation δ and the FWHM of a subspectrum.

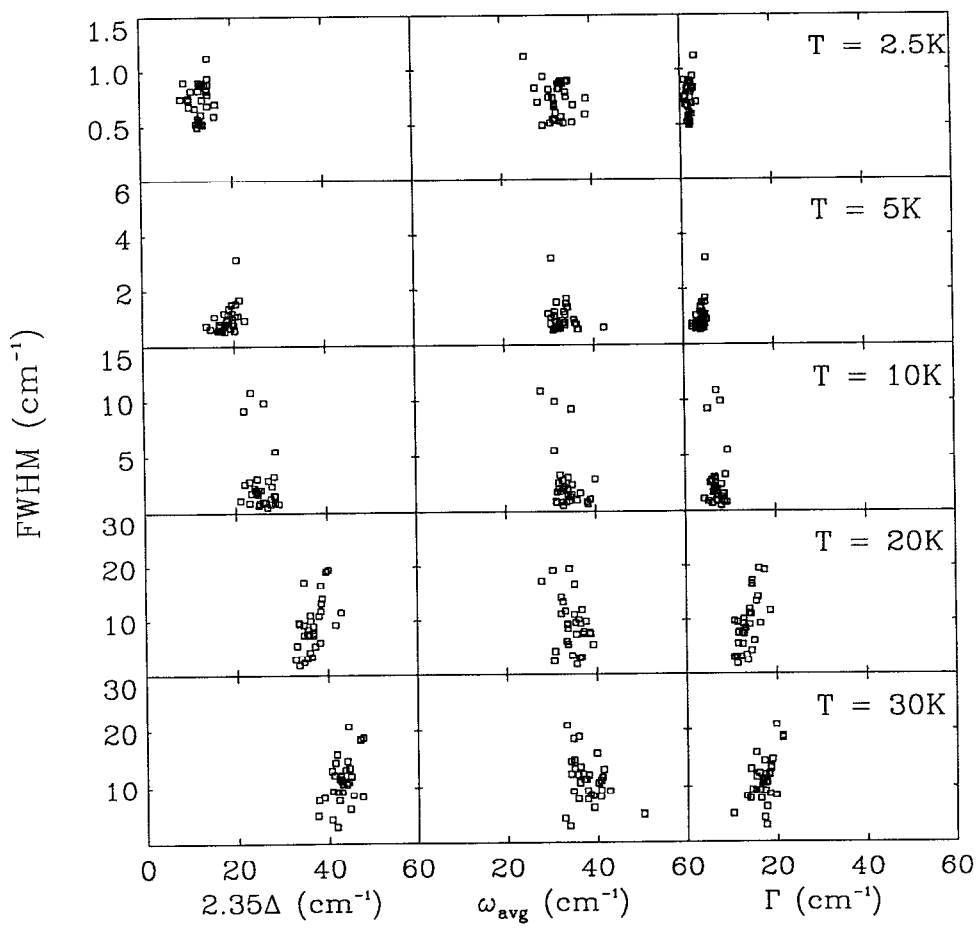

FIG. 11. Left column: the correlation between the rms fluctuation of $U(t)$ (Δ) and the FWHM of a subspectrum for the $N = 16$ cluster at various temperatures. Middle column: the correlation between the average frequency of the motion (ω_{avg}) and the FWHM of a subspectrum. Right column: the correlation between the Padé formula Γ for the FWHM and the calculated FWHM.

There is one other isomer found at this temperature which is somewhat less symmetric. The tight packing seen is typical of clusters at this temperature. The structure of the isomer may be described as seven hexagonal-packed Ar's above each side of the benzene, plus two Ar's along the edge of the benzene. The hexagonal packing along the side of the benzene is seen in all of the low temperature clusters for $N = 16$ and $N = 21$. We note that the benzene is not fully solvated; i.e., it is not completely surrounded by Ar atoms. This is due to the relatively low N value. The cluster at 30 K is highly asymmetric, and shows a much looser packing. The transition from tight to loose packing is typical of the solid to liquid transition in benzene–Ar clusters.

In Fig. 10 we show the correlation between the FWHM of the subspectra shown in Fig. 8 with the diffusion constant of the underlying trajectory. At 2.5 and 5 K the cluster is entirely solidlike and the diffusion constant of every initial condition in the thermal ensemble is zero. As the temperature is further increased, there is a *gradual* evolution of the diffusion constant to larger values. This gradual change of D with temperature is to be expected in a finite system. The finite size of these clusters is an important factor in understanding the solid to liquid phase transition. The trajectories sampled never show a bimodal distribution of D values, as a phase coexistence picture might suggest. Figure 10 also shows the correlation between the rms bond fluctuation δ and the FWHM of a subspectrum. According to the Lindemann criterion, liquidlike behavior is first found in these clusters at 20 K. Thus, δ becomes greater than 0.1 after very slow diffusive motion has begin to set in. At higher temperatures a correlation between δ and the FWHM appears.

In Fig. 11 we show the correlation between the FWHM and Δ. At 2.5, 5, and 10 K the width of the spectrum is not highly sensitive to Δ. This is predicted by an undamped oscillator model, and is a sign that harmonic motions are important at these temperatures. As the temperature is increased to 20 K, the FWHM becomes correlated with Δ but 2.35Δ is still a poor estimate for the FWHM. This is indicative of the motional narrowing paradigm (Case II). In the middle panel of Fig. 11 we also consider the correlation between the FWHM of the subspectra and ω_{avg}. To begin with, we note that the average frequency of the ensemble does not change significantly with temperature. This behavior may be rationalized by a harmonic oscillator model of the cluster. At 2.5 K the FWHM is not well correlated with ω_{avg} (with the possible exception of the broadest subspectrum). This is a characteristic of undamped, periodic motion. As the temperature is further increased the correlation between the FWHM and ω_{avg} improves. This is a sign of the system moving from the regime of periodic motion to the regime of motional narrowing.

The correlation between Γ [Eq. (24)] and the FWHM of a subspectrum is shown in the right panel of Fig. 11. The inclusion of dynamics in Γ leads to a much better estimator of the FWHM than the static approximation (Case III). At 5 K the Padé formula, while better than the static approximation, still overestimates the width of the narrow spectral features. This is because the motion is in Case I, where the

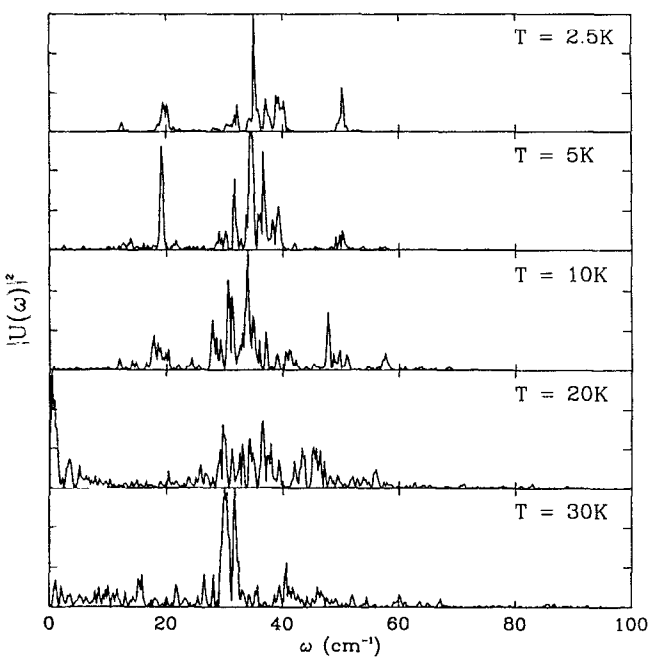

FIG. 12. The evolution $|U'(\omega)|^2$ functions based on a typical trajectory with temperature for the $N = 16$ cluster.

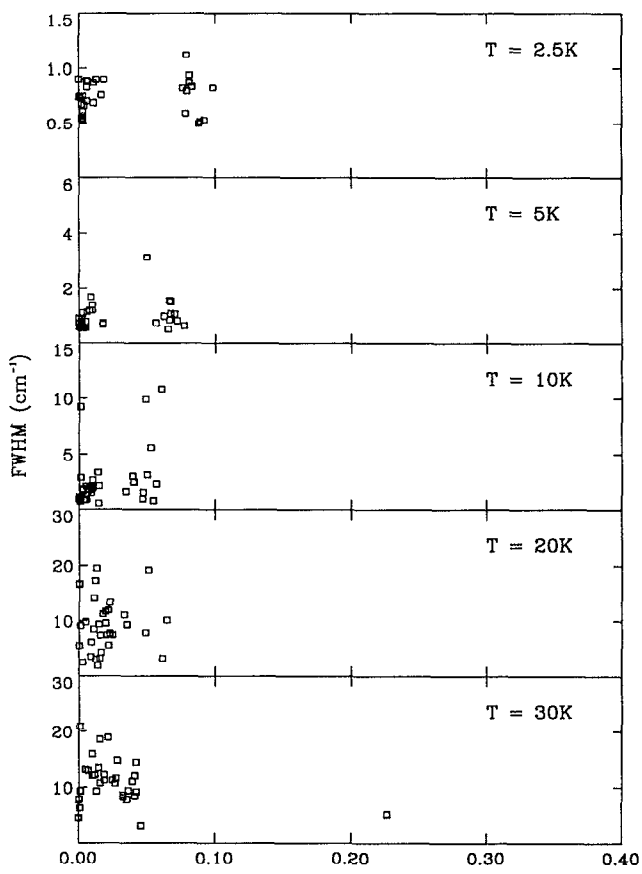

FIG. 13. Correlation between the asymmetry number and the FWHM of the subspectrum for the $N = 16$ cluster.

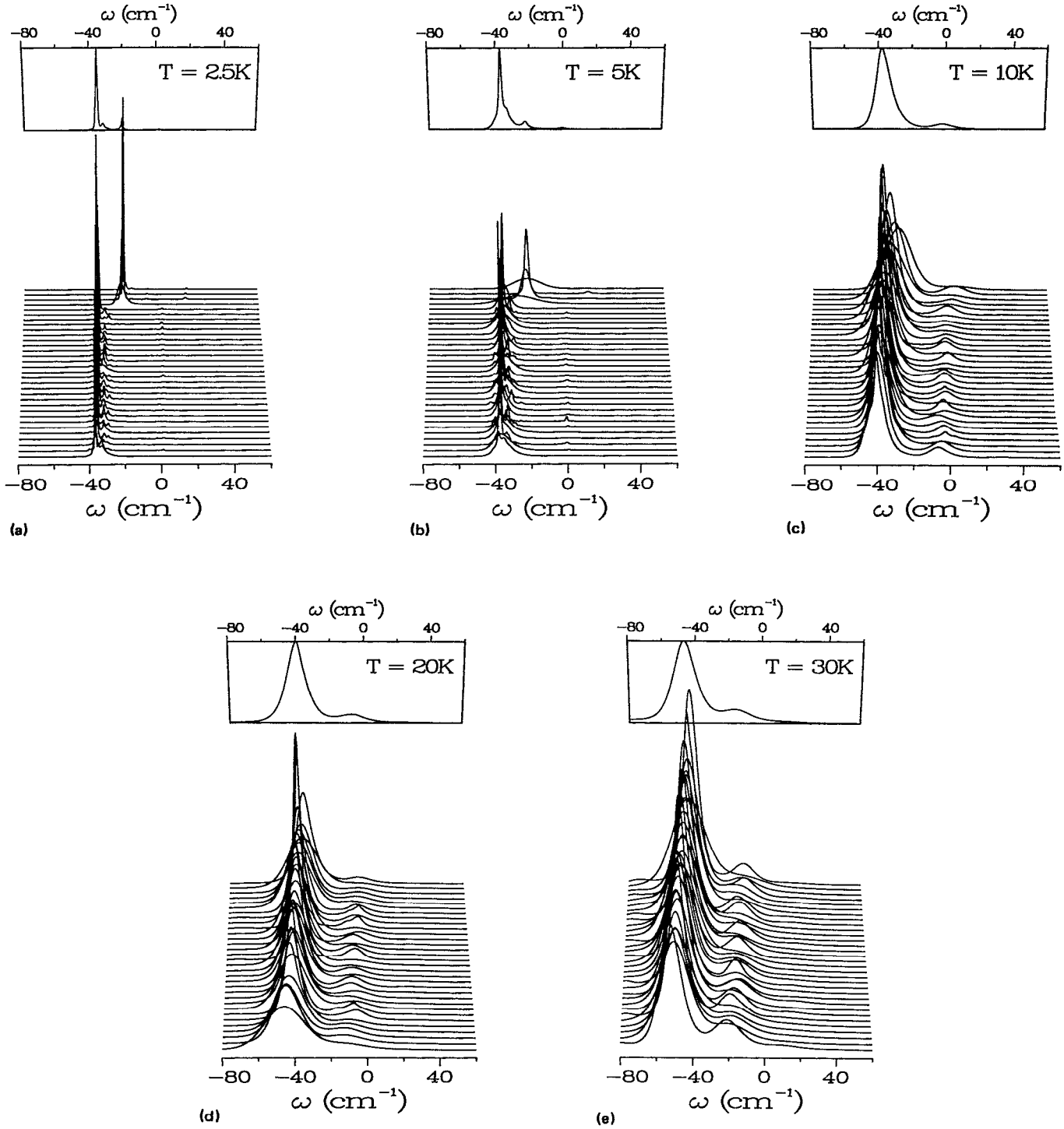

FIG. 14. Spectra and subspectra for the $N = 21$ cluster at various temperatures.

spectrum is narrow regardless of ω_{avg} and Δ. As the temperature is increased the system moves to Case II and Γ becomes a reasonably accurate predictor of the calculated FWHM.

Figure 12 shows typical $|U'(\omega)|^2$ for various temperatures. The figure shows that the spectroscopic change associated with the solid to liquid transition results from an increase in the number of excited modes, and an increase in the excitation of low frequency modes. At low temperatures relatively few modes are excited, and there is a clear gap between the first excited mode and zero frequency. This is indicative of a periodic $J_C(t)$ (Case I). As the temperature is increased, excitation of low frequency modes indicates that $J_C(t)$ will behave increasingly like a decaying function, and thus the system enters the Case II regime.

In Fig. 13 we show the correlation between the cluster

asymmetry number and the FWHM of a subspectrum. To begin with, note that highly asymmetric configurations are not very probable at any temperature. There is a slow decrease in the cluster asymmetry with increasing temperature. A more asymmetric isomer type ($z = 0.22$) is found at 30 K. This isomer has a very narrow absorption line shape. The reason for this may be that a significant portion of the Ar motions are decoupled from the chromophore. Less asymmetric cluster configurations do not seem to produce particularly narrow subspectra.

Before proceeding to calculations of the $N = 21$ clusters, let us summarize the main results of this section:

(1) As the temperature is increased, the $N = 16$ cluster undergoes a *gradual* transition from solidlike to liquidlike behavior. The smooth change in the average diffusion constant and δ with temperature is a due to the finite size of this system. As Adams and Stratt point out,[25] the inclusion of a chromophore in a rare gas cluster can enhance finite size effects. Another consequence of finite system size is that different properties (e.g., δ, D) predict different "melting" points.

(2) The spectroscopic manifestation of the melting transition is a move from a spectrum that behaves as if $J(t)$ were a periodic function (Case I) to a spectrum that behaves as if $J(t)$ were a decaying function (Case II). In the periodic regime the FWHM of the spectrum is insensitive to Δ and ω_{avg}. In the decaying regime the FWHM is positively correlated with Δ and negatively correlated with ω_{avg}. The Padé formula, which accounts approximately for motional narrowing, becomes more accurate as the temperature is increased.

(3) Sharp and narrow spectral features result from the interplay of structure and dynamics. Very narrow spectra can be caused by highly asymmetric isomers. Partially asymmetric isomers ($z < 0.2$) do not have especially narrow absorption spectra. The thermal ensemble of cluster configurations is dominated by nearly symmetric isomers at all the temperatures studied here.

D. Cluster spectra vs *T*: *N*=21

In this subsection we study the evolution of the cluster spectrum as a function of temperature for $N = 21$. The calculations and the following discussion are parallel to what we found for $N = 16$. Figure 14 shows the cluster absorption spectrum and associated subspectra for temperatures varying between 2.5 and 30 K. None of the clusters dissociated during the 140 ps simulation. At 2.5 K each subspectrum consists of a sharp line with a small amount of vibrational structure. At 5 K the cluster spectrum has two dominant peaks; one centered at about $-38\ cm^{-1}$, and the other centered at about $-20\ cm^{-1}$. It is apparent from the subspec-

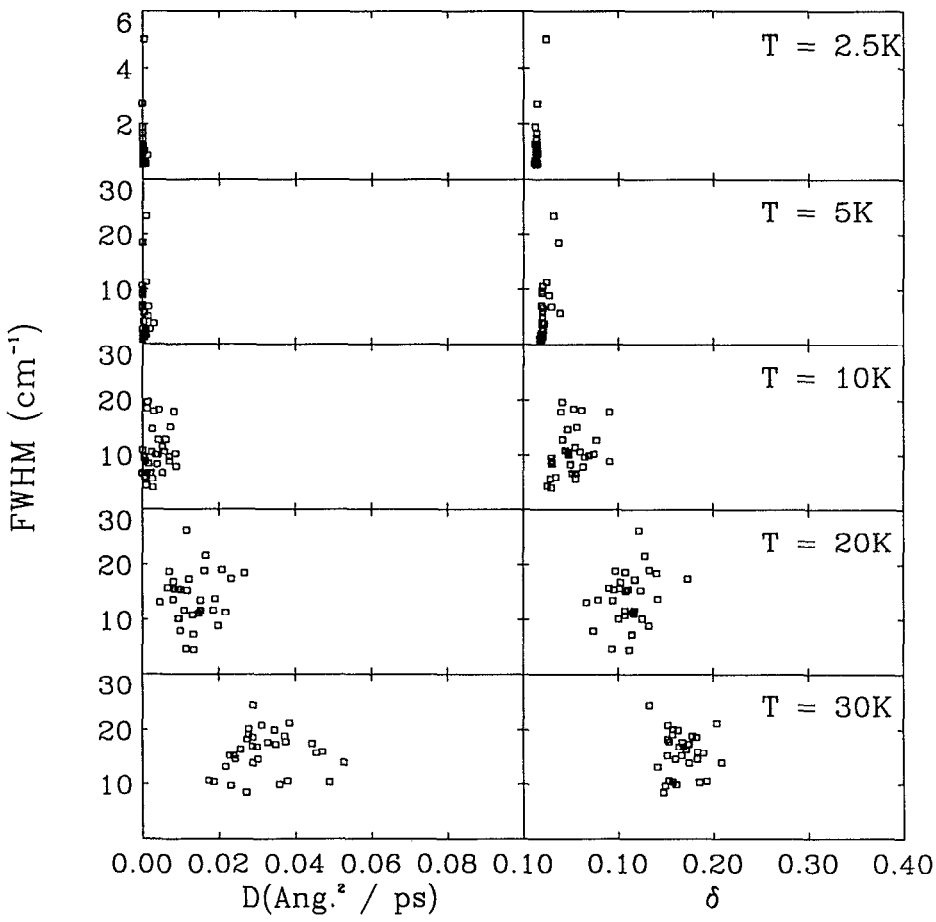

FIG. 15. Indicators of the solid–liquid transition for the $N = 21$ cluster. Left column: correlation between the cluster diffusion constant D and the FWHM of a subspectrum. Right column: correlation between the rms bond fluctuation δ and the FWHM of a subspectrum.

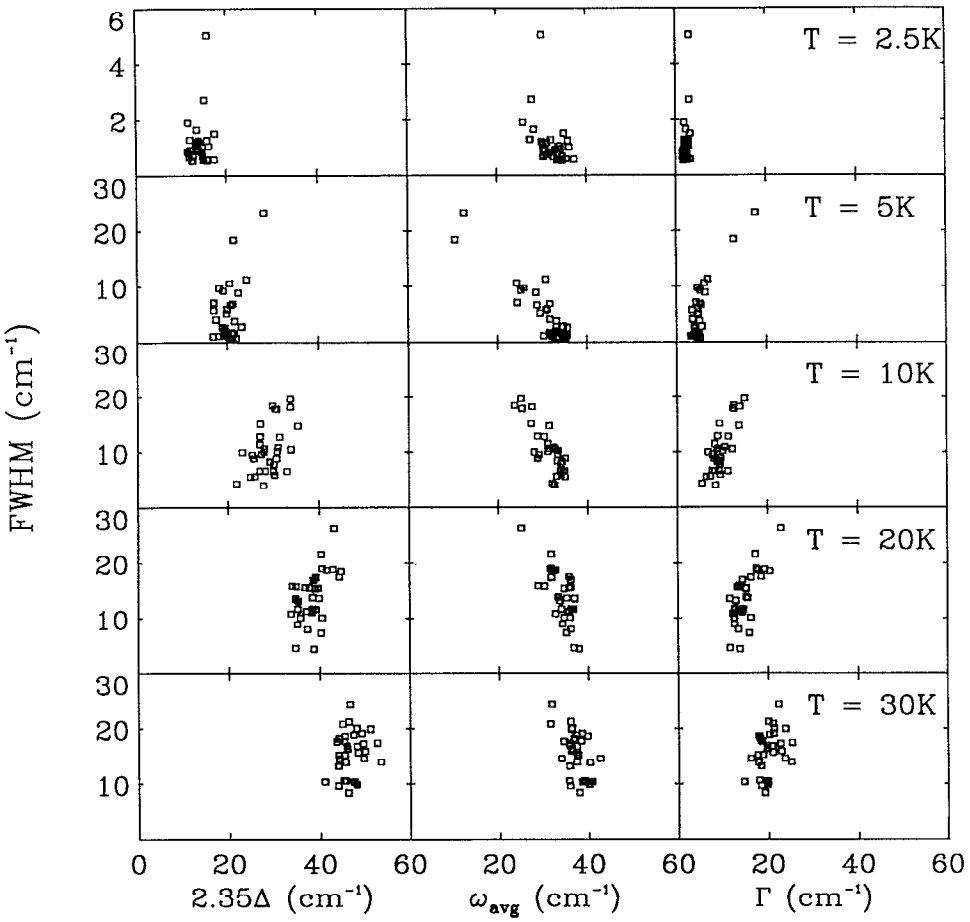

FIG. 16. Left column: the correlation between the rms fluctuation of $U(t)$ (Δ) and the FWHM of a subspectrum for the $N=21$ cluster at various temperatures. Middle column: the correlation between the average frequency of the motion (ω_{avg}) and the FWHM of a subspectrum. Right column: the correlation between the Padé formula Γ for the FWHM and the calculated FWHM.

tra that these sharp features are due to different isomers. Other broader subspectra occur with a variety of spectral shifts. As the temperature is further increased to 20 K the feature at -20 cm^{-1} disappears. Sharp subspectra (FWHM <5 cm^{-1}) still exist at 20 K. These subspectra are responsible for the sharpness of the main peak in the spectrum. At 30 K the subspectra begin to look more alike and sharp subspectra have disappeared entirely.

Let us now consider the dynamics underlying this spectroscopic behavior. In Fig. 15 we show the correlation between the FWHM of a subspectrum and D. As with the $N=16$ cluster, there is a gradual evolution of the diffusion constant as the temperature increases, which is indicative of the very small size of the system. There never occurs a temperature where the absorption of nondiffusive isomers is significantly narrower than the absorption of diffusive isomers within the thermal ensemble. For instance, the two sharpest subspectra at 20 K have nonzero diffusion constants. There is no clear correlation between the FWHM and D at any temperature. This is contrary to the $N=16$ cluster, where there was a better correlation between the FWHM and D.

Figure 15 also shows the correlation between the FWHM of a subspectra and δ. According to the Lindemann criterion, the clusters do not melt until 20 K. This is in agreement with our previous observations that some diffusive clusters are observed before δ increases to more than 0.1. The correlation of the FWHM with δ improves as the temperature is increased, but remains weak. This is in accord with the picture of a transition from Case I to Case II.

Figure 16 gives the correlation between the FWHM of a subspectrum and Δ. At low temperatures this correlation is poor, which is consistent with periodic motion. At higher temperatures the correlation improves. Thus, the solid to liquid transition in these clusters is accompanied by the spectroscopic transition from a periodic $J(t)$ (Case I) to a damped $J(t)$ (Case II). Figure 16 also shows the correlation between ω_{avg} and the FWHM of a subspectrum. At 2.5 and 5 K, two populations of subspectra appear; one that has the FWHM correlated with ω_{avg}, and one where the FWHM is uncorrelated with ω_{avg}. This is suggestive of a coexistence of isomers with periodic $J(t)$ values and other isomers with damped $J(t)$ values. As the temperature is increased from 5 to 10 K the undamped population disappears. Finally, we note that the slope of the correlation increases as the temperature is increased to 30 K. This is because the FWHM is proportional to Δ^2/ω_{avg}, and Δ^2 is increasing with T.

In the right panel of Fig. 16 we plot the correlation between Γ [Eq. (24)] and the FWHM of the subspectra. At 5 K we again see a manifestation of the bimodal distribution of trajectory types: clusters with broad FWHM are well corre-

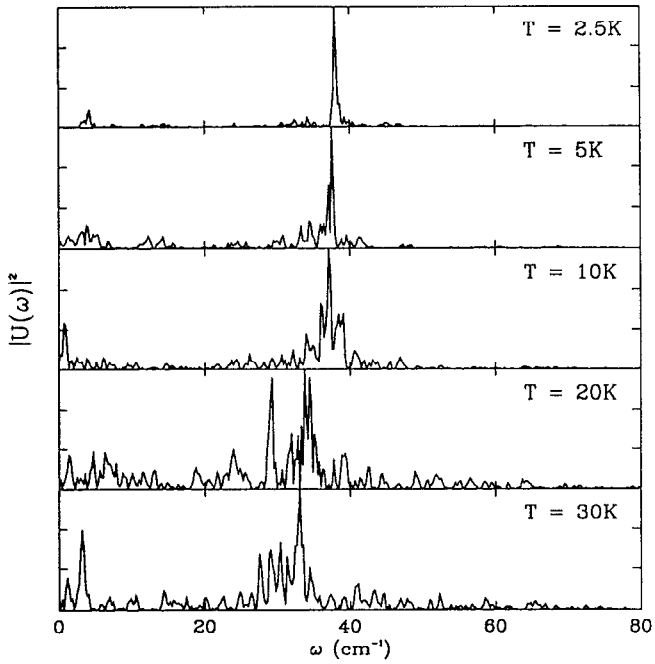

FIG. 17. The evolution of $|U'(\omega)|^2$ with temperature for the $N = 21$ cluster.

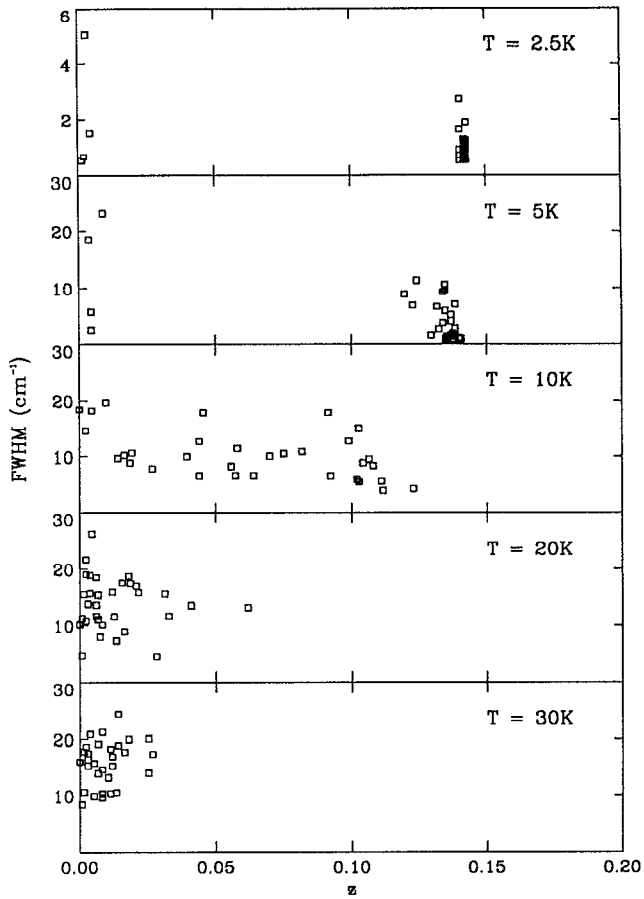

FIG. 18. The correlation between the asymmetry number z and the calculated FWHM for the $N = 21$ cluster.

lated with Γ whereas clusters with narrower FWHM have a much weaker correlation. As the temperature is increased to 10, 20, and 30 K Γ does a striking job of predicting the calculated FWHM. This indicates that the model of a decaying $J_C(t)$ is good away from very low temperatures. In Fig. 17 $|U'(\omega)|^2$ functions generated from typical trajectories are shown at various temperatures. At 2.5 K there is a pronounced gap between $\omega = 0$ and the first peak of $|U'(\omega)|^2$. This is characteristic of the Case I regime. As the temperature is increased a peak near $\omega = 0$ occurs. This signifies the transition to a decaying $J_C(t)$ (Case II).

In Fig. 18 we show the correlation between the FWHM and the asymmetry number z. At 2.5 K and 5 K there are two very probable isomers; one with zero asymmetry and the other with an asymmetry near 0.15. As the temperature is increased to 10 K side-crossing events occur, causing a broad distribution of z values. As with the $N = 16$ clusters, asymmetry does not play a significant role in producing broad or narrow spectral features. One exception to this is when $T = 30$ K. In this case there is a noticeable negative correlation between z and the FWHM. The probable explanation for this is that more symmetric clusters are less floppy than asymmetric clusters.

Figure 19 shows two typical cluster configurations from the $N = 21$ ensemble at 2.5 and 30 K. The configuration at 2.5 K has z very close to 0. It is tightly packed, and highly symmetric. The benzene is fully solvated, in the sense that it is fully surrounded by Ar atoms. Thus, benzene–Ar clusters undergo a transition from partially solvated to fully solvated configurations as N is increased from 16 to 21. The spectroscopic change accompanying this transition is a broadening of the main peak. The configuration at 30 K is much more loosely packed, and displays a preponderence of Ar atoms on one edge of the benzene. The degree of benzene solvation, however, remains high.

Let us summarize the main conclusions of this subsection:

(1) The $N = 21$ cluster shows a gradual evolution of D and δ with temperature, much like the $N = 16$ cluster. The distribution of D and δ are unimodal at every temperature, making it difficult to distinguish phases based on these properties.

(2) Distinct subpopulations of isomers in the Case I and Case II regime occur at 5 K. The number of Case I isomers decreases as the temperature is increased.

(3) The double-peaked spectra seen at 2.5 and 5 K are due to dominant symmetric and partially asymmetric isomers. The $N = 21$ isomers are more symmetric than the $N = 16$ isomers. This may be the cause of the broadening of the sharp main peak as N is increased (rather than, for instance, a transition to more liquidlike behavior).

IV. CONCLUSIONS

In this paper, we have taken a detailed look at how cluster properties are reflected in the spectrum. Just as the terms liquid and solid can be useful in describing qualitative aspects of cluster motion, we have found the classification of

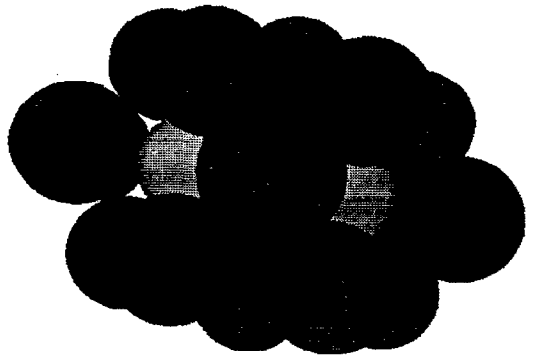

(a)

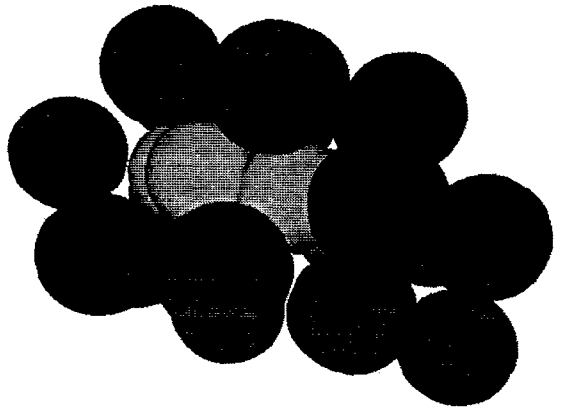

(b)

FIG. 19. Configurations for the $N = 21$ cluster at different temperatures: (a) 2.5 K, (b) 30 K.

the behavior of $J(t)$ into periodic, damped, and static behavior to be useful in describing the spectroscopic changes that occur as temperature or the number of Ar atoms are changed.

The different behaviors of $J(t)$ serve to explain many features of the observed spectra. For instance, isomers showing high frequency motions often have narrow absorption spectra. This is a result of motional narrowing. Other times, the FWHM of the isomer absorption is insensitive to the average frequency of the motion. This behavior is predicted by a periodic $J(t)$. We have also shown that oftentimes Δ [the rms fluctuation of $U(t)$] is a better predictor of the width of spectral features than the amplitude of cluster motion as reflected in δ. This is because Δ reflects the spectroscopically relevant part of cluster motion; it takes into account whether motions are uncoupled from the spectrum.

Another aim of this paper is to clarify the relation between cluster structure and the observed spectrum. Cluster asymmetry played a crucial role in producing the double peaked spectra found at $N = 1$, 2, and 4. Cluster asymmetry is less important for the larger clusters at 20 K. The importance of cluster asymmetry underlines the role the chromophore has in determining cluster structure, dynamics, and spectra for the N values considered here.

Finally, the question of how phase transitions occur in rare gas clusters containing a chromophore is still open. We have found that as N is varied at 20 K, benzene–Ar clusters undergo a transition from a solid ($N = 1,2$), to a 2D liquid ($N = 4$), to a 3D liquid ($N = 10,16,21$). The labels solid and liquid, however, must be used with great caution. Benzene–Ar clusters show a great deal of nonbulk behavior for the N values studied here. The addition of the benzene to the cluster slows the transition to bulk behavior as N is increased. For instance, the transitions we see in δ and the diffusion constant are quite gradual, even when compared to neat rare gas clusters of comparable size.

One important manifestation of finite cluster size is that different measures of solid or liquid can lead to ambiguity. For instance, as the temperature is increased for $N = 16$ or $N = 21$ the diffusion constant of some isomers becomes nonzero before δ gets bigger than 0.1. We explain this observation by noting that D can become nonzero if there is a wandering motion of any Ar atom, whereas δ reflects the overall amplitude of the cluster motion. Direct observations of the trajectories has led us to conclude that Ar atoms bound to the edge of the benzene tend to wander before the cluster melts as a whole.

In this paper we have described the effect of cluster structure and dynamics over a 140 ps time scale on the linear absorption spectrum. Work in progress shows that nanosecond hopping between isomers can occur. From the viewpoint of linear absorption, this hopping is indistinguishable from an inhomogeneous distribution of isomers. Nonlinear spectroscopies, however, can study such motions directly.[35] This points out the important need to probe phase transitions in clusters via nonlinear techniques such as hole burning[30] and photon echo spectroscopies.[31,40]

ACKNOWLEDGMENTS

The support of the National Science Foundation, the Air Force Office of Scientific Research, and the Petroleum Research Fund, administered by the American Chemical Society, is gratefully acknowledged. We also thank Cray Research, Inc., for providing a grant of computer time through the NSF Center for Photoinduced Charge Transfer which made the present calculations possible. Laurence E. Fried acknowledges the support of the NSF Postdoctoral Fellowship in Chemistry.

[1] M. L. Alexander, M. A. Johnson, N. E. Levinger, and W. C. Lineberger, Phys. Rev. Lett. 57, 976 (1986).

[2] S. Leutwyler and J. Bösiger, Chem. Rev. **90**, 489 (1990).
[3] J. Bösiger and S. Leutwyler, Phys. Rev. Lett. **59**, 1895 (1987); J. Bösiger, R. Knochenmuss, and S. Leutwyler, *ibid.* **62**, 3058 (1989).
[4] M. Hahn and R. Whetten, Phys. Rev. Lett. **61**, 1190 (1988).
[5] M. Hahn, Doctoral dissertation, University of California, Los Angeles, 1989.
[6] U. Even, N. Ben-Horin, and J. Jortner, Phys. Rev. Lett. **62**, 140 (1989); Chem. Phys. Lett. **156**, 138 (1989).
[7] G. Rajagopal, R. Barnett, A. Nitzan, U. Landman, E. Honea, P. Labastie, M. L. Homer, and R. L. Whetten, Phys. Rev. Lett. **64**, 2933 (1990).
[8] M. Schmidt, M. Mons, and J. Le Calvé, Chem. Phys. Lett. **177**, 371 (1991); M. Mons, J. Le Calvé, F. Piuzzi, and I. Dimicoli, J. Chem. Phys. **92**, 2155 (1990); M. Schmidt, M. Mons, J. LeCalvé, P. Millié, and C. Cossart-Magos, Chem. Phys. Lett. **183**, 69 (1991).
[9] A. Penner, A. Amirav, J. Jortner, A. Nitzan, and J. Gersten, J. Chem. Phys. **93**, 147 (1990).
[10] F. H. Stillinger and T. A. Weber, J. Chem. Phys. **81**, 5095 (1984).
[11] R. S. Berry, Sci. Am. **263**, 68 (1990).
[12] R. S. Berry, J. Jellinek, and G. Natanson, Phys. Rev. A **30**, 919 (1984).
[13] F. G. Amar and R. Berry, J. Chem. Phys. **85**, 5943 (1986).
[14] J. Jellinek, T. L. Beck, and R. S. Berry, J. Chem. Phys. **84**, 2783 (1986); T. L. Beck and R. S. Berry, *ibid.* **88**, 3910 (1988).
[15] T. L. Beck, D. M. Leitner, and R. S. Berry, J. Chem. Phys. **89**, 1681 (1988).
[16] D. J. Wales and R. S. Berry, J. Chem. Phys. **92**, 4283 (1990).
[17] T. Beck, J. Doll, and D. Freeman, J. Chem. Phys. **90**, 5651 (1989).
[18] D. L. Freeman and J. D. Doll, Adv. Chem. Phys. **70**, 139 (1988).
[19] S. Leutwyler, Chem. Phys. Lett. **115**, 40 (1985).
[20] J. C. Kettley, T. F. Palmer, J. P. Simons, and A. T. Amos, Chem. Phys. Lett. **126**, 107 (1986).
[21] H. C. Longuet-Higgins and J. A. Pople, J. Chem. Phys. **27**, 192 (1957).
[22] E. Shalev, N. Ben-Horin, and J. Jortner, Chem. Phys. Lett. **177**, 161 (1991).
[23] N. Ben-Horin, U. Even, and J. Jortner, J. Chem. Phys. **91**, 331 (1989).
[24] N. Liver, A. Nitzan, and J. Jortner, J. Chem. Phys. **88**, 3516 (1988).
[25] J. E. Adams and R. M. Stratt, J. Chem. Phys. **93**, 1358 (1990).
[26] L. E. Fried and S. Mukamel, Phys. Rev. Lett. **66**, 2340 (1991).
[27] J. D. Doll, D. L. Freeman, and M. J. Gillan, Chem. Phys. Lett. **143**, 277 (1988).
[28] R. Islampour and S. Mukamel, Chem. Phys. Lett. **107**, 2391 (1984); J. Chem. Phys. **80**, 5487 (1984).
[29] M. Ondrechen, Z. Berkovitch-Yell, and J. Jortner, J. Am. Chem. Soc. **103**, 6586 (1981).
[30] R. Knochenmuss and S. Leutwyler, J. Chem. Phys. **92**, 4686 (1990).
[31] Y. J. Yan and S. Mukamel, J. Chem. Phys. **94**, 179 (1991).
[32] For example, see R. N. Barnett, U. Landman, and A. Nitzan, J. Chem. Phys. **91**, 5567 (1989); P. J. Rossky and J. Schnitker, J. Phys. Chem. **92**, 4277 (1988).
[33] N. Bloembergen, E. M. Purcell, and R. V. Pound, Phys. Rev. **73**, 679 (1948).
[34] S. Mukamel, Ann. Rev. Phys. Chem. **41**, 647 (1990).
[35] J. Jellinek and D. H. Li, Phys. Rev. Lett. **62**, 241 (1989).
[36] M. P. Allen and D. J. Tildesley, *Computer Simulation of Liquids* (Oxford Science Publications, Oxford, 1987).
[37] J. Sue, Y. J. Yan, and S. Mukamel, J. Chem. Phys. **85**, 462 (1986).
[38] S. Kirkpatrick, C. D. Gelatt, Jr., and M. P. Vecchi, Science **220**, 671 (1983).
[39] W. H. Press, B. P. Flannery, S. A. Teukolsky, and W. T. Vetterling, *Numerical Recipes* (Cambridge University, Cambridge, 1986).
[40] L. E. Fried and S. Mukanel, Phys. Rev. Lett. (submitted).